Université de Montréal

# Détermination d'abondances d'éléments lourds dans la photosphère d'étoiles naines blanches riches en hélium

par

Stéphanie Desharnais

Département de physique

Faculté des arts et des sciences

Mémoire présenté à la Faculté des études supérieures

en vue de l'obtention du grade de

Maître ès sciences (M.Sc.)

en physique

Avril, 2007

Université de Montréal

Faculté des études supérieures

Ce mémoire intitulé:

Détermination d'abondances d'éléments lourds dans la photosphère d'étoiles naines blanches riches en hélium

présenté par:

Stéphanie Desharnais

a été évalué par un jury composé des personnes suivantes:

| | |
|---|---|
| Pierre Bergeron, | président-rapporteur |
| François Wesemael, | directeur de recherche |
| Nicole St-Louis, | membre du jury |

Mémoire accepté le: 26/04/07

# Sommaire

Le spectre visible des étoiles naines blanches de type DB est dominé par l'hélium neutre. Dans ce mémoire, nous présentons les résultats d'une analyse détaillée des spectres dans l'ultraviolet lointain de cinq naines blanches froides appartenant à cette classe spectrale. Les spectres à haute résolution des étoiles G270-124, GD 233, GD 61, GD 378 et GD 408 ont été obtenus en utilisant le satellite FUSE. Ces spectres montrent des transitions associées à différents états d'ionisation d'éléments lourds, notamment, le carbone, l'oxygène, le silicium, le fer ainsi que le soufre.

Avant de contraindre ou de déterminer les abondances de ces éléments, nous devons d'abord déterminer les paramètres atmosphériques fondamentaux de nos étoiles, c'est-à-dire, la température effective, la gravité de surface et l'abondance d'hydrogène. Pour ce faire, nous avons utilisé des spectres visibles de notre échantillon d'étoiles et modelisé les flux émergents dans les régions rouge (autour de la raie H$\alpha$) et bleue du visible.

Les abondances d'éléments lourds présents dans la photosphère de nos objets s'expliquent en terme d'une compétition entre un vent stellaire, le tri gravitationnel, l'accrétion de matière interstellaire (et circumstellaire), ainsi qu'un dragage convectif. Nos résultats permettent de clarifier l'importance relative des divers mécanismes physiques qui régissent l'évolution des naines blanches riches en hélium.

*Mots clefs:*

G270-124 – GD 233 – GD 61 – GD 378 – GD 408 – Naines blanches – DB – Carbone – Métaux – FUSE

# Abstract

We present a comprehensive analysis of the far-ultraviolet spectra of five DB white dwarfs spanning the effective temperature range between 15,040 K and 21,800 K. Atmospheric parameters were redetermined using a least-square fitting technique based on a Levenberg-Marquard algorithm and blue and red optical spectra. The FUSE line analysis shows that carbon features, observed in several hot DB stars at or above 22,000 K, are present in the two coolest (GD 408 and GD 378) and in the hottest (G270-124) target. In addition, four of the five objects display photospheric lines of silicon. Other heavy elements such as oxygen, iron and sulphur are also observed in some objects. The variations of the heavy element abundances as a function of effective temperature in DB stars are interpreted in terms of a competition between a stellar wind, gravitational settling, accretion from interstellar (and circumstellar) matter and convective dredge-up.

*Subject headings:*

G270-124 – GD 233 – GD 61 – GD 378 – GD 408 – White dwarf – DB – Carbon – Metals – FUSE

# *Table des matières*

**Sommaire** i

**Abstract** ii

**Table des matières** iii

**Liste des figures** v

**Liste des tableaux** vi

**1 Introduction** 1

**2 Article** 8

2.1 Abstract . . . . . 8

2.2 Introduction . . . . . 9

2.3 Observations . . . . . 12

2.3.1 Target selection . . . . . 12

2.3.2 FUSE data . . . . . 13

2.3.3 Optical data . . . . . 14

2.4 Model atmospheres . . . . . 15

2.5 Determination of atmospheric parameters . . . . . 16

2.6 Results of abundance analyses . . . . . 18

2.6.1 Carbon . . . . . 18

2.6.2 Oxygen . . . . . 20

2.6.3 Silicon, iron and sulphur . . . . . 20
2.6.4 Other heavy elements . . . . . 23
2.7 The pattern of heavy elements in DB stars . . . . . 23
2.8 Concluding remarks . . . . . 28
2.9 Acknowledgements . . . . . 29

**3 Tableaux et Figures** **30**

**4 Conclusion** **51**

**A Transitions d'éléments lourds** **53**

**Bibliographie** **56**

**Remerciements** **60**

# *Liste des figures*


3.1 Smoothed FUSE spectra of our five targets . . . . . 35

3.2 Smoothed FUSE night-time data of our five stars . . . . . 36

3.3 Blue and red spectra of our five target stars . . . . . 37

3.4 The region around the resonance doublet C II $\lambda$1036.337, $\lambda$1037.018 for our five stars . . . . . 38

3.5 Fits to the carbon feature detected in the FUSE spectrum of G270-124 . . . . . 39

3.6 Fits to the carbon features detected in the FUSE spectrum of GD 378 . . . . . 40

3.7 Fits to the weak carbon feature detected in the FUSE spectrum of GD 408 . . 41

3.8 The region around the triplet O I $\lambda$1039.230, $\lambda$1040.943, $\lambda$1041.688 in night-time data of the five stars . . . . . 42

3.9 Fits to the O I line $\lambda$1152.151 . . . . . 43

3.10 The region around the Si III complex $\lambda$1108.358, $\lambda$1109.970, $\lambda$1113.204 for our five stars . . . . . 44

3.11 Fits to the resonance triplet Si III $\lambda$1108.358, $\lambda$1109.970, $\lambda$1113.204 . . . . . 45

3.12 Fits to the Si II complex $\lambda$989.873, $\lambda$992.683, $\lambda$992.696 . . . . . 46

3.13 Fits to Fe II and Fe III transitions . . . . . 47

3.14 Fits to Fe II transitions . . . . . 48

3.15 Fits to the sulphur features detected in the FUSE spectrum of GD 378 . . . . . 49

3.16 Observed carbon abundances in helium-rich white dwarfs . . . . . 50

# *Liste des tableaux*

1.1 Couverture en longueurs d'onde des segments de FUSE. . . . . 7

3.1 Log of FUSE Observations . . . . . 30

3.2 Transitions of heavy elements of photospheric origin observed in cool DB white dwarfs (Cross X indicates a detection) . . . . . 31

3.3 Abundances in Cool DB White Dwarfs . . . . . 32

3.4 Relative abundances in Cool DB White Dwarfs . . . . . 33

3.5 Upper limits on the abundances of heavy elements . . . . . 34

A.1 Transitions d'éléments lourds observées dans la photosphère de naines blanches froides de type DB . . . . . 54

# *Chapitre* 1

# Introduction

Les étoiles naines blanches représentent la phase ultime du cheminement évolutif de la majorité des étoiles. En effet, les étoiles possédant une masse inférieure à $\sim 8\ M_{\odot}$ (ce qui représente plus de 95% des étoiles composant la Voie Lactée) termineront leur vie sous forme de naine blanche. La structure physique de ces étoiles diffère de celle des étoiles de la séquence principale, puisque la densité moyenne de l'étoile est suffisamment élevée pour que les effets quantiques y deviennent importants: la matière est alors dite "dégénérée". C'est justement la pression due aux électrons dégénérés qui empêche la naine blanche de s'effondrer sous l'effet de sa propre gravité. Avec 99% de la masse de la naine blanche concentrée dans le noyau, seule une faible fraction de la masse restante, constituant la photosphère de l'étoile, est accessible par observation.

Cette mince enveloppe stellaire représente une source essentielle d'information. En effet, la température de surface des naines blanches couvre un large éventail de valeurs et est un signe de l'évolution de l'étoile puisque, à ce stade, la fusion nucléaire a cessé et la naine blanche doit sa faible luminosité au lent refroidissement de son cœur. Le taux de refroidissement dépend de la taille du réservoir thermique des ions non-dégénérés ainsi que du taux de transfert d'énergie au travers de l'enveloppe isolante. Une fois son réservoir thermique épuisé, la naine blanche cessera de rayonner et deviendra une naine noire.

La composition chimique de la photosphère des naines blanches diffère d'un type spectral à un autre. La nomenclature utilisée afin de les différencier est expliquée par Wesemael et

al. (1993). En effet, environ 2/3 de toutes les étoiles naines blanches montrent uniquement des raies d'hydrogène dans leur spectre visible. Ces étoiles sont classifiées DA et ont été généralement bien étudiées au cours des dernières années. Une plus faible fraction, moins de 20%, est caractérisée par un spectre visible dominé par l'hélium neutre et une composition chimique dominée par l'hélium qui inclut peu ou pas d'hydrogène. Ces naines blanches sont de type spectral DB, et on retrouve la grande majorité d'entre elles dans un intervalle de températures effectives entre 30,000 K et environ 13,000 K. En raison de leur rareté et de leur magnitude apparente plus faible, les propriétés de ces objets restent relativement moins bien connues que celles des étoiles de type DA. Certaines étoiles de type DB montrent parfois des traces d'hydrogène et sont baptisées DBA, alors que d'autres ont des raies d'éléments lourds, tel le calcium, et sont de type spectral DBZ.

La borne froide des DB est expliquée par le fait que les raies de l'hélium neutre, dont la présence définit cette classe spectrale, deviennent invisibles pour des températures plus faibles que 13,000 K. Du côté chaud, les raies d'hélium neutre persistent jusqu'au delà de 50,000 K (Dreizler & Werner 1996). On pourrait donc s'attendre à ce que la distribution des étoiles de type DB soit le prolongement de celle des étoiles DO, dont le spectre est dominé par les raies d'hélium ionisé. L'analyse récente des naines blanches riches en hélium contenues dans le sondage SDSS montre cependant que la région entre 30,000 K et 45,000 K, même si elle n'est pas vide d'étoiles riches en hélium comme on le pensait il n'y a pas si longtemps, reste peu peuplée. Globalement, on y retrouve deux fois moins d'étoiles que ce qui serait attendu sur la base du nombre d'étoiles DB en deça de 30,000 K (Eisenstein et al. 2006). Il est probable que le mécanisme suggéré par Fontaine & Wesemael (1987) pour expliquer le faible nombre d'étoiles riches en hélium entre 45,000 K et 30,000 K reste d'actualité. Il est basé sur l'idée que, dans certaines étoiles de type DO, une faible quantité d'hydrogène localisée profondément dans l'enveloppe pourrait diffuser en surface, de sorte qu'une étoile de type DO de 50,000 K deviendrait de type DA à 40,000 K. La convection dans la zone d'hélium sous-jacente, qui diluerait subséquemment la mince couche d'hydrogène en surface, permettrait la ré-émergence d'étoiles riches en hélium à plus faible température effective, de l'ordre de 30,000 K.

La pureté de la photosphère d'une étoile de type spectral DB est principalement liée à

l'efficacité du tri gravitationnel dans son atmosphère et son enveloppe. Les naines blanches sont caractérisées par un champ gravitationnel intense ($\log g \sim 8$) et nous nous attendons donc à ce que l'hydrogène, l'élément chimique le plus léger, flotte à la surface de l'étoile tandis que les éléments plus lourds coulent dans les couches plus profondes. Ce raisonnement suggère que les naines blanches de type DB naissent avec très peu ou pas d'hydrogène, l'hélium étant alors l'élément le plus léger et l'élément dominant. La composition de la photosphère d'une DB représente encore aujourd'hui un défi à expliquer en faisant appel à un minimum de mécanismes physiques.

La présence d'impuretés dans l'atmosphère des étoiles riches en hélium implique l'existence d'autres processus physiques qui entrent en compétition avec le tri gravitationnel et les uns avec les autres. Pour expliquer les abondances des éléments dominants et des éléments traces dans la photosphère d'une étoile, on doit considérer plusieurs processus.

Parmi ceux-ci, on retrouve la diffusion de l'hydrogène provenant de stades évolutifs antérieurs, le mélange convectif lié à la recombinaison de l'hélium et le processus d'accélération radiative permettant la lévitation sélective d'éléments lourds. Les éléments lourds observés dans la photosphère des naines blanches proviendraient de sources externes. L'explication la plus répandue demeure à ce jour l'accrétion de matière à partir du milieu interstellaire selon le scénario en deux phases d'accrétion/diffusion de Dupuis et al. (1992, 1993a, b). Cependant, ce modèle présente certains problèmes, par exemple, l'absence de corrélation spatiale entre les étoiles et le gaz interstellaire local (Aanestad et al. 1993; Zuckerman et al. 2003), et de récentes observations suggèrent que l'accrétion serait continue selon des taux variant avec les conditions du milieu ambiant (Koester et al. 2005; Koester & Wilken 2006). De plus, Jura (2006) propose que, dans le cas de certaines naines blanches riches en hélium montrant une sous-abondance de carbone, les faibles valeurs du rapport d'abondance $N(\mathrm{C})/N(\mathrm{Fe})$ mesurées s'expliqueraient par de l'accrétion à partir de matière circumstellaire ayant une composition chondritique plutôt qu'à partir de matière interstellaire.

Contrairement aux autres éléments lourds, le carbone proviendrait du cœur même de l'étoile. Toutefois, sa présence demeure difficile à expliquer dans le cadre des modèles classiques d'évolution spectrale. L'hypothèse de l'existence d'un faible vent stellaire s'opposant au tri

gravitationnel pour les étoiles DB chaudes ($T_{\rm eff} > 20,000$ K) a été discutée par différents auteurs (Fontaine & Brassard 2005; Petitclerc et al. 2005). Ce vent serait un résidu des forts vents stellaires que l'on retrouve dans les précurseurs des étoiles DB et serait cohérent avec une évolution spectrale PG 1159 → DO → DB des naines blanches riches en hélium (Unglaub & Bues 2000). Afin de rendre compte des observations d'abondances de carbone dans la photosphère des étoiles plus froides ($T_{\rm eff} < 20,000$ K), on fait appel à un modèle théorique de dragage convectif. Le carbone issu des couches profondes de l'étoile est ramené à la surface au fur et à mesure que la base de la zone convective s'enfonce dans l'enveloppe stellaire et s'approche du coeur de carbone (Koester et al. 1982; Fontaine et al. 1984). L'efficacité de ce mécanisme est maximale à des températures effectives inférieures à 13,000 K (Pelletier et al. 1986; MacDonald et al. 1998).

Le but de ce projet est de mettre en relief l'importance de ces différents mécanismes en présentant une analyse de la composition chimique de l'atmosphère des naines blanches de type DB. En observant la présence (ou encore l'absence) d'éléments lourds dans la photosphère de ces étoiles, puis en contraignant leurs abondances, nous sommes en mesure de poursuivre le travail de compréhension des phénomènes physiques présents dans les couches externes des naines blanches de type DB.

Le télescope spatial FUSE (Far Ultraviolet Spectroscopic Explorer) s'avère un outil indispensable dans le cadre de notre étude. En effet, la région spectrale ultraviolette couverte par le satellite (905 à 1187 Å) en est une où l'on retrouve de nombreuses transitions associées à des éléments lourds. Lancé par la NASA le 24 juin 1999 et géré par *The Johns Hopkins University*, le satellite FUSE circule sur une orbite quasi circulaire de 768 km de rayon (Moos 2000). Sa principale mission est d'observer le deutérium présent dans l'univers dans le cadre du programme *Origins* de la NASA, en obtenant des données spectroscopiques de haute résolution ($R \equiv \lambda/\Delta\lambda$, entre 12000 et 30000) dans le domaine de l'ultraviolet lointain. Sa mission initiale de 3 ans a toutefois été reconduite deux fois, et FUSE a entrepris sa huitième année d'activité en 2007. FUSE permet d'obtenir des données pour trois dimensions de diaphragme, auxquelles correspondent trois résolutions différentes. Pour une résolution maximale, on utilise le diaphragme HIRS ($1.25'' \times 20''$); pour une résolution moyenne, le diaphragme MDRS ($4'' \times 20''$)

tandis que l'ouverture la plus fréquemment utilisée, LWRS (30″ × 30″), permet l'observation d'objets peu brillants comme les naines blanches.

Le satellite lui-même mesure environ 5.5 m de long et possède une masse de près de 1360 kg. Il inclut quatre miroirs paraboliques de 387 × 352 $mm^2$, d'une longueur focale de 2245 mm. Deux miroirs sont recouverts de carbure de silicium (SiC) et permettent la réflexion aux courtes longueurs d'onde ultraviolettes. Ces canaux SiC offrent une meilleure efficacité pour des longueurs d'onde inférieures à ∼1020 Å. Les deux autres miroirs sont recouverts de flurorure de lithium (LiF) sur une couche d'aluminium et réfléchissent les longueurs d'onde ultraviolettes plus longues. Ces canaux LiF montrent une efficacité jusqu'à deux fois supérieure à celle des canaux SiC pour des longueurs d'onde plus grandes que 1050 Å. Puisque les sections efficaces des différents miroirs varient avec la longueur d'onde, certains canaux présentent un meilleur rapport signal sur bruit selon la région spectrale considérée.

À chaque miroir correspond un réseau de diffraction gravé par holographie et corrigé pour l'astigmatisme. Ces réseaux sont gravés sur un substrat courbé de façon à produire quatre spectrographes circulaires de Rowland de 1652 mm de diamètre. La lumière ultraviolette dispersée est detectée par deux plaques à microcanaux (MCP). La surface de ces détecteurs est courbée afin d'être compatible avec la courbure du plan focal. Chaque détecteur est également divisé en deux segments indépendants, A et B, séparés par une petite brèche en longueur d'onde. Afin de s'assurer que les brèches ne soient pas aux mêmes longueurs d'onde pour les deux détecteurs, ceux-ci sont légèrement décalés l'un par rapport à l'autre. Le Tableau 1.1 indique la plage de longueurs d'onde couverte pour chaque détecteur. Les quatre canaux couvrent la région 1015-1075 Å. Le pic d'efficacité de FUSE se situe aux alentours de 1050 Å.

L'analyse des spectres ultraviolets obtenus avec le satellite FUSE nous permet de mesurer les abondances d'éléments lourds observés dans la photosphère des naines blanches qui composent notre échantillon ou alors d'imposer une limite sur ces abondances lorsque l'élément est absent. Avant de procéder, nous devons cependant obtenir les paramètres atmosphériques de nos objets, c'est-à-dire, la température effective, la gravité de surface ainsi que l'abondance d'hydrogène. Pour ce faire, nous avons obtenu des spectres dans les régions bleue et rouge du visible pour nos cinq étoiles, à l'exception de l'objet le plus froid de notre échantillon, GD 408,

pour lequel nous avons uniquement en notre possession le spectre visible bleu. Les données observationnelles dans la partie rouge du spectre, autour de la raie H$\alpha$, ont été recueillies au Kitt Peak National Observatory, alors que les spectres bleus ont été obtenus au Steward Observatory de l'Université de l'Arizona. En utilisant une méthode itérative, nous avons, tour à tour, modélisé le spectre bleu afin d'obtenir une première approximation de la température et de la gravité de surface, puis nous avons utilisé ces résultats afin de contraindre l'abondance d'hydrogène en modélisant la raie H$\alpha$ dans le spectre rouge. La procédure a été répétée jusqu'à la convergence satisfaisante des paramètres fondamentaux. Dans le cas particulier de GD 408, nous avons pu uniquement nous baser sur une modélisation du spectre bleu et sur les contraintes imposées par la raie H$\beta$.

Une fois les paramètres atmosphériques établis, nous avons obtenu les abondances d'éléments en utilisant une grille de modèles d'atmosphères calculés à l'aide du code d'atmosphère de l'Université de Montréal (Beauchamp 1995) et une grille de spectres synthétiques obtenus à l'aide de la version 43 du code SYNSPEC (Hubený & Lanz 1995).

TABLEAU 1.1 – Couverture en longueurs d'onde des segments de FUSE.

| Canal | Segment A | Segment B |
|---|---|---|
| SiC 1 | 1090.9 – 1003.7 | 992.7 – 905.0 |
| LiF 1 | 987.1 – 1082.3 | 1094.0 – 1187.7 |
| SiC 2 | 916.6 – 1005.5 | 1016.4 – 1103.8 |
| LiF 2 | 1181.9 – 1086.7 | 1075.0 – 979.2 |

# *Chapitre* 2

# Article

## FUSE Observations of Heavy Elements in the Photospheres of Cool DB White Dwarfs[1]

S. Desharnais, F. Wesemael

*Département de physique, Université de Montréal, C.P. 6128, Succ. Centre-Ville, Montréal, QC H3C 3J7, Canada*

stephanie, wesemael@astro.umontreal.ca

P. Chayer, and J.W. Kruk

*Bloomberg Center for Physics and Astronomy, The Johns Hopkins University, Baltimore, MD 21218, USA*

chayer, kruk@pha.jhu.edu

### 2.1 Abstract

We present a comprehensive analysis of the far-ultraviolet spectra of five DB white dwarfs spanning the effective temperature range between 15,040 K and 21,800 K. The FUSE line analysis shows that carbon features, previously observed in several hot DB stars at or above 22,000 K, are present in the two coolest (GD 408 and GD 378) and in the hottest (G270-124) target. The observed carbon abundances range from $\log N(\mathrm{C})/N(\mathrm{He}) \sim -6.9$ to $\sim -7.8$. In

[1]FUSE is operated by the Johns Hopkins University under NASA contract NAS 5-32985

addition, four of the five objects display photospheric lines of silicon. Other elements such as oxygen, iron and sulphur are also observed in some objects. The variations of the abundances of heavy elements as a function of effective temperature in DB stars are interpreted in terms of a competition between a stellar wind, gravitational settling, accretion from interstellar (and circumstellar) matter and convective dredge-up.

## 2.2 Introduction

Because of their relative rarity and of their faintness, the small fraction (less than 20 %) of white dwarfs that show strong neutral helium lines in their optical spectra and no or very little hydrogen, the DB stars, have been less amenable to detailed analyses than their more numerous hydrogen-line (DA) counterparts. Until recently, the DB stars were thought to be restricted to the effective temperature range between 13,000 K and 30,000 K, while the DO white dwarfs, with optical spectra dominated by the lines of ionized helium, are observed above 40,000 K. No DB stars with an effective temperature between 45,000 K and 30,000 K was known to exist, a range known as the DB gap. More recent observations of the DB stars included in the Sloan Digital Sky Survey now show several well-observed stars populating the gap (Eisenstein et al. 2006), although there remains a dearth of stars in the $40,000 - 25,000$ K interval compared to the numbers observed between 22,000 K and 16,000 K. The sparsity of stars at the hot end of the DB range is traditionally accounted for by spectral evolution in the outer layers of cooling helium-rich white dwarfs (Fontaine & Wesemael 1987). On the low temperature side, the disappearance of DB stars is simply due to the disappearance of neutral helium lines at effective temperatures below 13,000 K.

The purity of the photospheres of DB white dwarfs is closely linked to the efficiency of downward gravitational settling. In the photosphere of a white dwarf, it is generally expected that hydrogen, the lightest element, will float at the top of the atmosphere while heavy elements will sink into deeper layers. This mechanism suggests that DB stars are born with no or very little hydrogen, and that helium is the lightest element present in the photosphere. The traces of hydrogen seen in those DB stars that display weak Balmer or Lyman lines of hydrogen, the DBA stars (Shipman et al. 1987), are likely to be accreted (Liebert et al. 1987).

There are also other types of impurities seen in the atmospheres of some DB degenerates, namely traces of heavy elements. In the optical, ionized calcium is fairly common in the so-called DBZ or DBAZ stars, while lines of other heavy elements, such as carbon, magnesium, silicon and iron are occasionally seen in the ultraviolet (see, e.g., Shipman & Greenstein 1983; Wegner & Nelan 1987; Friedrich et al. 1999).

The presence of these elements implies that other physical processes, besides gravitational settling, are at work in the stellar envelope and photosphere of DB stars, and that all these processes compete with each other. Indeed, to account satisfactorily for the abundance patterns of trace elements, we need to call upon several additional mechanisms. In the hotter helium-rich degenerates (DO stars and the very hottest DB stars), it is likely that radiative element support plays a role, but its effectiveness in maintaining measurable traces of heavy elements decreases rapidly in DB stars. At the low end of the temperature scale, it is likely that some of the heavy elements observed, such as calcium, are extrinsic and accreted by the star from external sources. The most palatable idea is that the heavy elements are accreted from the interstellar medium. This idea has been discussed in detail in the framework of a two-phase model of the interstellar medium by Dupuis et al. (1992, 1993a, b). However, there are persistent problems with this scenario (Aanestad et al. 1993; Zuckerman et al. 2003), and recent observations appear to favor continuous — rather than episodic — accretion with rates varying with the conditions of the ambient medium (Koester et al. 2005, Koester & Wilken 2006). In addition, more exotic sources of heavy elements have been considered occasionally: Alcock et al. (1986) rely on comets that originate from an Oort-like cloud, while Jura (2006) argues that the abundance ratio $N(\mathrm{C})/N(\mathrm{Fe})$ in some helium-rich white dwarfs could be accounted for by accretion from matter with a chondritic composition, perhaps similar to that found in asteroids.

Carbon is of particular interest in the helium-rich white dwarfs, as it is perhaps moke likely that its reservoir is located in the stellar core rather than in interstellar space. In helium-rich stars below 30,000 K, this element is observable in three distinct contexts; *i)* in the form of C I lines or broad molecular Swan bands in the optical spectra of the DQ stars, restricted to effective temperatures between approximately 6000 K and 11,000 K (see Dufour et al. 2005

for a recent analysis and a review of the relevant litterature); *ii)* as narrow transitions of C I in the ultraviolet spectra of cool DC stars, those helium-atmosphere white dwarfs below 13,000 K that display a continuous optical spectrum (Wegner 1981, 1983a); *iii)* as transitions of neutral and ionized carbon in the ultraviolet spectra of DB stars between 13,000 K and 30,000 K (Wegner & Nelan 1987; Provencal et al. 2000; Petitclerc et al. 2005).

In the cool DQ and DC white dwarfs, the presence of carbon is thought to be associated with convective dredge-up, the process by which convection brings back to the surface carbon dredged-up from the equilibrium diffusion tail at the helium-carbon interface (Koester et al. 1982; Fontaine et al. 1984). The efficiency of this process is expected to decrease significantly at effective temperatures above 13,000 K, the approximate temperature above which the helium convection zone becomes too shallow for large quantities of carbon to be brought back to the photosphere (Pelletier et al. 1986; MacDonald et al. 1998). Nevertheless, dredge-up could well account for the carbon observed in stars between 13,000 K and 19,000 K, a regime where the theoretical predictions have never really been confronted with observations. At the other end, in the very hottest DB stars as well as in the DO stars, radiative element support, together perhaps with stellar winds and gravitational settling, may play a role in accounting for the observed abundances. It is, however, in the intermediate-temperature objects, above approximately 19,000 K, that the presence of carbon is the most difficult to account for. In this intermediate temperature range, neither radiative forces nor dredge-up are likely to be up to the task of maintaining abundance ratios even as low as $N(\mathrm{C})/N(\mathrm{He}) \sim 10^{-7}$ in the photosphere. Fontaine & Brassard (2005) were the first to suggest that the carbon found in the photospheres of those DB stars is left over from previous evolutionary phases, but is prevented from completely settling out of view by a weak wind. This wind, which currently has no firm physical basis, could be a remnant of those found in the precursors of the DO and DB white dwarfs, the very hot ($T_{\mathrm{eff}} > 80{,}000$ K) PG 1159 stars (Unglaub & Bues 2000). These ideas were taken up by Petitclerc et al. (2005), who applied them to a small sample of DB stars hotter than 22,000 K observed with the FUSE satellite. While this model appears to be a promising way to account for the handful of carbon abundances measured up to now in hot DB stars, much remains to be done on the observational side. Clearly, the investigation initiated by

Provencal et al. (2000) and taken up by Petitclerc et al. (2005) deserves to be extended to a larger sample of objects. The new Far Ultraviolet Spectroscopic Explorer (FUSE) observations we present in this paper allow us to make some headway in this direction.

This paper is structured as follows: The observational material which forms the basis of our investigation is presented in § 2.3, while § 2.4 presents the model atmospheres we rely on to provide atmospheric parameters and element abundances for our stars. We present, in § 2.5, our analysis of the blue and red optical spectra of our targets, while the abundances of trace elements seen in the FUSE data and their origin are determined and discussed in § 2.6 and 2.7. Our concluding remarks are presented in § 2.8.

## 2.3 Observations

### 2.3.1 Target selection

We initiated several years ago a project to document the abundances of heavy elements in DB stars with the help of the FUSE satellite. The first results of this project were presented by Petitclerc et al. (2005) and subsequent progress reports can be found in Wesemael et al. (2006) and Desharnais et al. (2007).

In the present contribution, we provide a detailed analysis of five additional DB stars. The objects were chosen on the basis of their apparent brightness and effective temperature, both of which determine the ultraviolet flux. Since our main goal is to extend the analysis of Petitclerc et al. (2005) to cooler temperatures, our targets are fairly bright DB stars in the range between 21,000 K and 15,000 K. The three coolest objects studied are GD 408, GD 378 and GD 61. The former is a DBZ star with $V = 14.33$, while the other two are DBAZ stars at visual magnitudes of $V = 14.39$ and $V = 14.86$, respectively. The low hydrogen abundance of GD 408 was first discussed by Weidemann & Koester (1991), and all three objects were included in the samples of Greenstein (1984), Oke et al. (1984), Sion et al. (1988), as well as in the important spectroscopic study of Wegner & Nelan (1987). These last authors derive upper limits on their carbon abundance on the basis of the absence of C I transitions in low-dispersion IUE spectra. The radial velocities are discussed by Aanestad et al. (1993) and the

recalibrated IUE spectra of GD 408 and GD 378 were later reanalyzed by Wolff et al. (2002) in order to extend the carbon abundance analysis to other heavy elements. In addition, the detection of silicon in GD 61 was reported by Wesemael et al. (2006).

The fourth star, GD 233 ($V = 14.52$), has been discussed less extensively. The atmospheric parameters of this DBA white dwarf were determined by Koester et al. (1981), Oke et al. (1984) and Wegner & Nelan (1987). The last object of our sample is the DBA white dwarf G270-124. With its visual magnitude of $V = 13.89$, it is the brightest and hottest of our targets. It appears in the photometric analysis of Wegner (1983b) and in the spectroscopic studies of Oke et al. (1984), Liebert et al. (1986) and Wegner & Nelan (1987). Along with GD 408 and GD 378, G270-124 is also featured in the ultraviolet archives of Bica et al. (1996) and Holberg et al. (2003). The IUE spectra of all three stars were recently analyzed by Castanheira et al. (2006) who redetermined the atmospheric parameters on that basis.

### 2.3.2 FUSE data

The FUSE detectors span the ultraviolet region between 905 and 1187 Å, a region where numerous weak transitions associated with heavy elements are located. The spectroscopic observations were secured in TTAG mode through the high-throughput LWRS aperture, which provides high-resolution ultraviolet spectra with $\lambda/\Delta\lambda \sim 15{,}000$. Three objects, GD 378, GD 61 and GD 233, were observed within GO program D168, a fourth one — the cool star GD 408 — through GO program G062, while the data for the fifth target, G270-124, were secured by one of us (JWK) within the FUSE photometric calibration program M102. A detailed log of the FUSE observations is presented in Table 3.1. The FUSE observations typically consist of one (GD 61, GD 233, GD 408) or two (GD 378, G270-124) series of exposures. Data are reduced using the pipeline software CALFUSE (version 3.0.4 for all stars save GD 408 for which version 3.1 was used). The individual exposures were coadded for segments *a* and *b* for the four channels (SiC1, SiC2, LiF1 and LiF2) individually. All eight segments were then coadded in order to produce a final spectrum covering the whole FUSE spectral range. To carry out this procedure, we use the publicly available program FUSE_register written by Lindler (2001). Channels were coadded by using a linear interpolation between the spectra

and by using scalar weights based on the exposure times. Spectra were edited to remove bad data such as endpoint data or the abnormal flux level variation, the so-called 'worm', in the LiF1b segment. Ultraviolet spectra generated in this way for our five target stars are shown in Figure 3.1. For the spectral analysis, we combine the segments that provide the best resolution after accounting for the small wavelength shifts between them. The procedure is particularly helpful in the case of the cool star GD 408, whose spectrum is less well exposed than those of the other targets. In all cases, the noise level varies throughout the spectrum. This is due to the significant change in the effective area of the channels with wavelength, which results in variations in the signal-to-noise ratio. In addition, the number of segments covering a given spectral region is a function of wavelength.

When searching for weak lines of heavy elements, it is useful to isolate the "night-only data", secured when the emission from the geocorona is minimal. The procedure was already used by Petitclerc et al. (2005), and is carried out here as well for all five targets. Data are reduced using the latest version of the CALFUSE pipeline (version 3.2) and night data are extracted using the IDF screen script for faint objects. Further details are provided by the IDF Cookbook (Goddard 2004). In the case of G270-124, only the night-time data of the second set of exposures are considered. The observations for the first set of exposures have a total integration time of roughly 400 s, but the pipeline calculates the exposure times for exposures number 3 and 4 in an erroneous manner. By using an IDF file, we are able to divide the night data into the eight usual FUSE segments (SiC1a, SiC1b, SiC2a, SiC2b, LiF1a, LiF1b, LiF2a and LiF2b). These segments are then coadded with FUSE_register, as was previously done for the combined day and night observations. Figure 3.2 shows the night-time data only for all five targets.

### 2.3.3 Optical data

In order to derive $T_{\rm eff}$, $\log g$ and the hydrogen abundance of our five targets, we use optical spectra secured earlier on. The blue optical data were obtained in the course of a program of observations of DB stars at the University of Arizona Steward Observatory with the 2.3-meter Bok Telescope equipped with a 800 x 800 TI or a 1200 x 800 Loral CCD. The setup

consists of a Boller and Chivens Spectrograph, a 4.5″ slit width and a 600 lines/mm grating is used in first order. This combination provides a spectral coverage of $\sim$ 3750-5100 Å at a resolution of $\sim$ 6 Å and a signal-to-noise ratio varying between 55 and 80. Observations of the red H$\alpha$ region were conducted at the Kitt Peak National Observatory (KPNO) in 1999 and 2000. The instrumental setup includes the 4-meter Ritchey-Chretien Spectrograph with a Tektronix 2k×2k CCD. A grating with 790 lines/mm blazed at 9500 Å is used in first order. The slit width varies between 1.5″ and 3″ and the resulting spectra cover the wavelength range between 5800-7200 Å with FWHM $\sim$ 3 Å and a S/N ratio between 20 and 100. Figure 3.3 shows the blue and red spectra secured for each star. Note that we have no coverage of the H$\alpha$ line in the cool star GD 408.

## 2.4 Model atmospheres

The grid of models used in this investigation is based on a slightly updated version of the model atmosphere code used in the analysis of Beauchamp (1995). The models are in LTE, are line-blanketed, and include the transport of energy by convection. For consistency, the mixing-length theory was treated using a parameterization of $\alpha = 1.25$ (Fontaine et al. 1981), already used by Beauchamp (1995) and Beauchamp et al. (1999). The chemical composition includes only helium and hydrogen and no heavy elements. The model grid covers the effective temperature range between 13,000 K and 32,000 K, the log surface gravity range 7.5(0.5)9.0 (g·cm·s$^{-2}$) and the hydrogen abundance range log $N$(H)/$N$(He) = 2.5(0.5)6.5.

Once the temperature stratification is secured, a first synthetic spectrum code allows the detailed computation of the emergent flux in the optical range. The code includes a treatment of van der Waals broadening of the He I transitions and of the broadening of the He I lines due to resonance as well as of the opacity in the far ultraviolet ($\lambda < 950$ Å). It includes both quadratic and linear Stark effects, and treats the transition from impact to quasi-static broadening by the electrons, while the ions are always treated within the quasi-static approximation. For the line analysis in the ultraviolet, our approach is similar to that used by Petitclerc et al. (2005). We treat the heavy elements as trace species and use a second synthetic spectrum code, the public program SYNPLOT written by I. Hubený, for

that region. SYNPLOT calls SYNSPEC, version 43 (Hubený & Lanz, 1995), to calculate the LTE populations of the appropriate excitations and ionization states of heavy elements. SYNPLOT allows one to identify quickly the transitions of interest of numerous ions and determines the profiles of the lines associated with a given trace species from the line list available on the SYNSPEC website[2]. All synthetic spectra in the ultraviolet were calculated by assuming a rotational velocity $v \sin i = 0$, since there is currently no evidence for significant rotation velocities in hot DB stars (Dufour et al. 2002; Petitclerc et al. 2005). To match the instrumental resolution of the FUSE observations, we convolve the synthetic spectra in the ultraviolet with a Gaussian of full width at half maximum of 0.06 Å.

## 2.5 Determination of atmospheric parameters

Our starting point for the determination of the atmospheric parameters of our five targets is the work of Beauchamp (1995), who determined atmospheric parameters for a large sample of DB stars. We use an improved $\chi^2$ fitting procedure based on a Levenberg-Marquard algorithm (Press et al. 1992) to compare the He I (and H I) line profiles with synthetic spectra associated with atmospheres with various H/He ratios. While double (hot and cool) solutions are frequent, it is generally easy to judge the best fit among the solutions found. Indeed, one of the two solutions generally fits the data quite satisfactorily, while the other shows a much poorer agreement. Blue optical spectra can be used to determine (in DBA stars) or constrain (in DB stars) the hydrogen abundance on the basis of the H$\beta$ line. However, for four of our targets, red optical spectra are also available, and we were able to use an iterative procedure to constrain the hydrogen abundance based on the presence or the absence of H$\alpha$. Typically, we start with the effective temperature and surface gravity determined from the blue spectrum, together with a first estimate of the H/He ratio. The H/He ratio is then refined on the basis of the H$\alpha$ line at the fixed values of $T_{\rm eff}$ and $\log g$. With that improved abundance, the blue spectrum is again fitted to determine corrected values of $T_{\rm eff}$ and $\log g$. The procedure is repeated until it converges to the desired accuracy, typically 10 K in effective temperature, 0.001 dex in $\log g$ and 0.01 dex in log (H/He).

[2]http://nova.astro.umd.edu/Synspec43/data/gfFUV99.dat.gz

For G270-124, we find a result that differs from that of Beauchamp (1995) who fits this object on the basis of a helium-pure atmosphere. Our observations (Figure 3.3) clearly show a weak H$\alpha$ transition, and G270-124 is reclassified a DBA white dwarf by Hunter et al. (2001) on the basis of that evidence. On that basis, we derive $T_{\rm eff} = 20,800 \pm 330$ K, log $g = 7.94 \pm 0.03$ and log (H/He) $= -4.68 \pm 0.08$, while Beauchamp (1995) derived 24,175 $\pm$ 437 K, log $g = 8.05 \pm 0.02$ with pure helium models. Our somewhat noisy red spectrum of GD 233 does not display a clear H$\alpha$ line, although some structure is obviously present. The blue spectrum of that star was fit with a pure helium atmosphere by Beauchamp (1995). However, the presence of the H$\alpha$ line was recently confirmed in the high-resolution UVES/VLT spectrum secured by Voss et al. (2007). Our fits give an effective temperature and surface gravity of $T_{\rm eff} = 18,410 \pm 100$ K and log $g = 8.03 \pm 0.03$, while our determination of the hydrogen abundance of log (H/He) $= -5.34 \pm 0.21$, is consistent with the value derived by Voss et al. (2007).

GD 61 is a DBAZ star and its red spectrum shows a strong H$\alpha$ line. We determine an effective temperature of $T_{\rm eff} = 17,340 \pm 90$ K, a surface gravity of log $g = 8.24 \pm 0.03$ and a hydrogen abundance of log (H/He) $= -3.97 \pm 0.02$. The effective temperature and hydrogen abundance that we derive are consistent with the results of Beauchamp (1995) as well as with the somewhat scattered values summarized in Sion et al. (1988), while we find a slightly higher surface gravity. For the DBAZ star GD 378, we determine $T_{\rm eff} = 16,700 \pm 70$ K, log $g = 8.09 \pm 0.04$, and a hydrogen abundance of log (H/He) $= -4.22 \pm 0.03$. Our temperature is roughly 1000 K hotter than that of Oke et al. (1984) who used multichannel data, 700 K higher than Sion et al. (1988), 500 K higher than Beauchamp (1995), but is compatible with the more recent determinations of Wolff et al. (2002).

As stated above, only a blue spectrum is available for GD 408. Based on the absence of H$\beta$, we can only provide a weaker constraint on the hydrogen abundance. Weidemann & Koester (1991) note the presence of a weak H$\alpha$ line in a red CCD spectrum of that object secured at the Calar Alto 3.5-m telescope. The cool solution based on the blue data available gives a relatively high value for the surface gravity. Our fit yields $T_{\rm eff} = 15,040 \pm 150$ K, log $g = 8.63 \pm 0.10$ and a limit on the hydrogen abundance of log (H/He) $< -5.20 \pm 0.26$ which is more

stringent than the limit determined by Sion et al. (1988) and consistent with the value of log (H/He) = −6 determined by Weidemann & Koester (1991). GD 408 was part of the analysis of Beauchamp (1995) in which he derived an effective temperature and a surface gravity of $T_{\rm eff}$ = 14,403 ± 84 K, log $g$ = 8.02 ± 0.05, based on a helium-pure atmosphere. Even if we consider an atmosphere pure in helium, our best fit gives a large surface gravity of log $g$ = 8.55 ± 0.08 (and $T_{\rm eff} = 15,160 \pm 120$). Our temperature is roughly 1000 K hotter than that of Weidemann & Koester (1991), based on multichannel spectrophotometry, and that of Wolff et al. (2002), based on the IUE spectrum and visual magnitude.

## 2.6 Results of abundance analyses

An examination of the FUSE spectra of our stars shows that numerous features of photospheric origin are observed in all five targets. Specifically, we detect narrow lines of carbon, oxygen, silicon, iron, and sulphur. A list of the observed transitions of photospheric origin is given in Table 3.2, while Table 3.3 shows our abundance determinations for these heavy elements, augmented with the calcium abundances determined for three objects by Sion et al. (1988). Finally, in Table 3.4, we show some relative abundances of interest. Let us now comment briefly on the individual elements analyzed.

### 2.6.1 Carbon

Photospheric carbon is not observed in the spectra of the cool stars GD 233 and GD 61. Since the second feature of the C II doublet λ1037.018 is absent of the observations, the observed λ1036.337 component is most likely of ISM origin only. We derive upper limits of log (C/He) < −8.8 and log (C/He) < −8.9 for these two stars, respectively. In the other three stars, the photospheric features previously seen in somewhat hotter DB stars by Petitclerc et al. (2005) are detected. Two lines were observed : the C II doublet λ1036.337, λ1037.018 and the C II complex λ1009.358, λ1010.083, λ1010.371. Figure 3.4 shows the region around the resonance doublet C II λ1036.337, λ1037.018 for our five targets. The FUSE spectrum of G270-124, the hottest star of our sample, displays only one of these transitions, namely the C II λ1036 doublet. An interstellar contribution is present, especially in λ1036.337, which originates

from the ground state. The $\lambda$1037.018 component has a weaker interstellar contribution as it originates on a level 63.4 $cm^{-1}$ above the ground state. We determine a carbon abundance of log (C/He) $= -7.8 \pm 0.1$, an abundance 25 to 250 smaller than that measured in the hotter DB stars observed by Provencal et al. (2000) and Petitclerc et al. (2005). Our fits to this carbon line are shown in Figure 3.5. At this low abundance, the C II $\lambda$1010 transition is not predicted by our synthetic spectra.

GD 378 shows the resonance doublet C II $\lambda$1036, 1037. The interstellar and photospheric components of $\lambda$1036.337 are well separated. In addition, the C II triplet $\lambda$1010, which originates from an excited level approximately 43,000 $cm^{-1}$ above the ground state, is present as well. Figure 3.6 shows our fits to these transitions. We determine a carbon abundance of log (C/He) $= -6.9 \pm 0.1$, which is consistent with the upper limit of log (C/He) $= < -5.5$ determined by Petitclerc et al. (2005) on the basis of low-dispersion IUE spectrum (Holberg et al. 2003), which had been previously analyzed by Wegner & Nelan (1987). At this abundance, our synthetic spectrum predicts a strong C I transition at $\lambda$1140.441. According to the line list we use (SYNSPEC gfFUV linelist), this line has its lower level 10,192.63 $cm^{-1}$ above the ground state and an $f$-value of $f = 0.530$. This line is not predicted in other databases we checked, where we found no evidence for a C I transition at that wavelength. Specifically, we consulted the NIST[3], Kelly[4] (1987) and Kentucky[5] databases as well as Wiese et al. (1966) and Kelly & Palumbo (1973). The C II doublet $\lambda$1036.337, $\lambda$1037.018 is also observed in the spectrum of our coolest star, GD 408. We fit the component originating on the excited level, $\lambda$1037.018 (Figure 3.7), and estimate a carbon abundance log (C/He) $= -8.7 \pm 0.2$, consistent with the upper limit of Petitclerc et al. (2005) and Wegner & Nelan (1987) of log (C/He) $= < -7.0$. Note that the determination of the carbon abundance in GD 378 and GD 408, are currently the only two available for DB stars below 21,000 K.

[3]http://physics.nist.gov/PhysRefData/ASD/index.html
[4]http://cfa-www.harvard.edu/amdata/ampdata/kelly/kelly.html
[5]http://www.pa.uky.edu/~peter/atomic/

### 2.6.2 Oxygen

By extracting the night-time data from the FUSE spectra, we are able to detect photospheric transitions associated with O I, an element which has not been seen previously in DB white dwarfs. Because the emission lines of geocoronal origin (Feldman et al. 2001) are considerably weaker in the night-only data, we were able to measure the abundance of oxygen in two targets and to set an upper limit on the oxygen abundance in the other three objects. Our spectra display four lines of O I. The complexes $\lambda$989 and $\lambda$1040 have components originating both from the ground state and from excited levels 158.265 and 226.977 $cm^{-1}$ above the ground state, while $\lambda$999 and $\lambda$1152 both have a lower level 15,867.862 $cm^{-1}$ above the ground state. Figure 3.8 shows the region around the triplet O I $\lambda$1039.230, $\lambda$1040.943, $\lambda$1041.688 for our five stars. The excited components of the O I triplet $\lambda$1040 are present in the FUSE spectrum of GD 61, as are the other excited lines $\lambda$999.497 and $\lambda$1152.151. The same features are observed in GD 378. In addition, the spectrum of GD 378 displays the O I complex at $\lambda$988.655, $\lambda$988.773, $\lambda$990.127, $\lambda$990.204 and $\lambda$990.801. The components $\lambda$988.655 and $\lambda$988.773 originate on the ground level while $\lambda$990.127, $\lambda$990.204 and $\lambda$990.801 have their lower level $> 158$ $cm^{-1}$ above the ground state. Figure 3.9 presents our fits to the O I $\lambda$1152 line. We determine an oxygen abundance of log (O/He) $= -6.0 \pm 0.2$ in GD 61 and log (O/He) $= -6.0 \pm 0.3$ in GD 378.

The spectra of the two hottest stars, G270-124 and GD 233, and that of the coolest star, GD 408, do not display photospheric oxygen features. In these cases, the $\lambda$1039.230 line, which originates from the ground state, is most likely of ISM origin. From the absence of the excited components of this triplet, $\lambda$1040.943 and $\lambda$1041.688, we were able to derive upper limits of log (O/He) $< -5.9$ in G270-124, log (O/He ) $< -6.2$ in GD 233 and log (O/He) $< -6.6$ in GD 408.

### 2.6.3 Silicon, iron and sulphur

Silicon is present in the form of the Si II $\lambda$992 transition and in the Si III complex $\lambda$1113. Figure 3.10 shows the region around the Si III triplet for all five targets. The discovery of the Si III $\lambda$1113 transitions in GD 61 had been reported by Wesemael et al. (2006). The Si

II and Si III features are present in the photospheres of G270-124, GD 61 and GD 378. The Si II triplet $\lambda$989.873, $\lambda$992.683, $\lambda$992.696 originates from both the ground state and from an excited fine-structure state 287.24 cm$^{-1}$ above the ground state. The Si III transitions $\lambda$1108.358, $\lambda$1109.970 and $\lambda$1113.230 must be of photospheric origin since they originate on a lower level approximately 53,000 cm$^{-1}$ above the ground state. Our fits to the Si III triplet $\lambda$1113 are shown for all three stars in Figure 3.11. We derive abundances of log (Si/He) = $-7.6 \pm 0.1$ in G270-124, log (Si/He) = $-6.7 \pm 0.2$ in GD 61, while we obtain log (Si/He) = $-7.2 \pm 0.1$ for GD 378. This last value is consistent with the upper limit determined by Wolff et al. (2002) in that object, log (Si/He) $< -6.5$, based on IUE spectroscopy. The FUSE spectrum of our coolest target GD 408 displays only the transitions associated with the Si II ion at $\lambda$992. We show our fits in Figure 3.12 along with the observations of and fit to GD 378. We determine log (Si/He) = $-8.0 \pm 0.4$ for GD 408 while Wolff et al. (2002) estimated an upper limit of log (Si/He) $< -8.0$. We found no evidence of silicon in the photosphere of GD 233, and derive an upper limit of log (Si/He) $< -8.0$ for that object.

Numerous lines associated with iron were also observed. The spectrum of G270-124 displays only the Fe III $\lambda$1122.526, $\lambda$1124.881 doublet. The component at 1122.526 Å originates from the ground state, while that at 1124.881 Å originates from a level 436.2 cm$^{-1}$ above the ground state and is likely to be of photospheric origin. The spectrum of GD 378 displays the same Fe III transitions. Our fits are presented in Figure 3.13 and are consistent with an abundance of log (Fe/He) = $-7.2 \pm 0.1$ for G270-124 and log (Fe/He) = $-7.3 \pm 0.2$ for the cooler star GD 378, in agreement with the upper limit of Wolff et al. (2002) (log (Fe/He) $< -5.5$). Based on the transitions of photospheric origin of carbon, silicon and iron observed in the FUSE spectrum of G270-124, we determine an average photospheric velocity of +36 km s$^{-1}$, while we estimate $v_{\rm ISM} = 0$ km s$^{-1}$ from the ISM N I triplet $\lambda$1134.165, $\lambda$1134.415, $\lambda$1134.980 and the O I $\lambda$1039.230 line observed in its night-time spectrum.

The ultraviolet spectrum of GD 233 shows no evidence of iron lines and an upper limit of log (Fe/He) $< -7.8$ was derived for this object. Since no heavy elements of photospheric origin were observed in this star, we could not determine the radial velocity. That derived by Greenstein & Trimble (1967), +40 km s$^{-1}$, is still relevant. We determine an average ISM

velocity of $v_{\rm ISM} = +3$ km s$^{-1}$ based on the presence of interstellar components of the C II $\lambda$1036.337, Si II $\lambda$1020.699 and O I $\lambda$1039.230 transitions as well as of the N I triplet $\lambda$1134.

The Fe III $\lambda$1122.526 transition in GD 61 is most likely of ISM origin. However, the FUSE spectrum also displays another feature : the Fe II lines $\lambda$1144.938, $\lambda$1147.409 and $\lambda$1148.277. The $\lambda$1144.938 component originates on the ground state, while the other two originate on excited levels 384.79 cm$^{-1}$ above the ground state. These Fe II lines were also detected in the two coolest targets, GD 378 and GD 408. Our fits are shown in Figure 3.14 and yield an abundance of log (Fe/He) $= -7.6 \pm 0.2$ in GD 61, log (Fe/He) $= -7.3 \pm 0.2$ in GD 378 and log (Fe/He) $= -8.0 \pm 0.2$ in GD 408, the latter is consistent with the value determined by Wolff et al. (2002), namely log (Fe/He) $= -7.5$ [+0.5; −1.0]. Based on the photospheric components of the transitions of oxygen, silicon and iron present in the spectrum of GD 61, we estimate an average radial velocity somewhat larger than that of +54 km s$^{-1}$ derived by Aanestad et al. (1993) on the basis of the H and K lines seen in MMT spectra. Specifically, we find +64 $\pm$ 4 km s$^{-1}$. Even if the N I $\lambda$1134 triplet appears weak in the night-time observations of GD 61, we were able to estimate $v_{\rm ISM} = +33$ km s$^{-1}$ based on its presence and on the ISM C II $\lambda$1036.337 line. As for GD 408, we use the photospheric components of the C II, Si II and Fe II transitions to measure an average photospheric velocity of +32 km s$^{-1}$, a value in very good agreement with the velocity of +34 km s$^{-1}$ derived by Aanestad et al. (1993). The ISM N I triplet $\lambda$1134 is not observed in the night-time spectrum of GD 408. We could only estimate an ISM velocity of $v_{\rm ISM} = +9$ km s$^{-1}$ based on the O I $\lambda$1039.230 transition of interstellar origin.

The ultraviolet spectrum of GD 378 is rich in iron lines. In addition to the transitions already discussed, we observe the Fe II lines at $\lambda$989.895, $\lambda$990.859, which are probably of photospheric origin since they originate on excited levels 1872.567 and 2430.097 cm$^{-1}$ above the ground state. Other features are present : the Fe II $\lambda$1063.176, $\lambda$1068.346, $\lambda$1071.584 and $\lambda$1075.635 transitions with the $\lambda$1063.176 line originating from the ground state and the $\lambda$1068.346, $\lambda$1071.584 and $\lambda$1075.635 lines originating from lower levels 384.79, 667.683 and 862.613 cm$^{-1}$ above the ground state, respectively, and the narrow Fe II transition $\lambda$1096.607 originating on a lower level 384.79 cm$^{-1}$ above the ground state.

Finally, the spectrum of GD 378 also shows narrow lines of sulphur. These S II transitions originate on excited levels $> 14,800$ cm$^{-1}$ above the ground state and are likely to be of photospheric origin. We detect the S II complex $\lambda$1014.110, $\lambda$1014.437, $\lambda$1019.528 as well as the S II transition $\lambda$1124.986. The low $f$-values of the first three transitions, $\log f = -2.600$, $-1.470$ and $-1.690$ respectively, based on the SYNSPEC linelist, could not account for the observations in GD 378. However, we found larger $f$-values for these transitions in the Kentucky database ($\log gf = -1.053$, $-0.0612$ and $-0.3187$). When we adopt the values extracted from the Kentucky database, our synthetic spectra are in good agreement with the observations. Figure 3.15 presents these regions along with our fits. We determine a sulphur abundance log (S/He) $= -7.7 \pm 0.1$. Based on the strongest lines associated with heavy elements observed in GD 378, we derive a photospheric velocity of +12 km s$^{-1}$, a value that differs from the velocity determined by Aanestad et al. (1993) on the basis of the H and K lines, +43 km s$^{-1}$. A velocity of $v_{\rm ISM} = -27$ km s$^{-1}$ was estimated from the ISM N I triplet $\lambda$1134 and from the shifted interstellar component in the doublet C II $\lambda$1036.

### 2.6.4 Other heavy elements

The ultraviolet region covered by the FUSE satellite is rich in transitions associated with heavy elements other than the ones we already discussed. Night-time data allow us to secure limits on the abundance of nitrogen whose features are usually contaminated by geocoronal emission lines. We also secure upper limits on the following additional heavy elements : P, Cl, Ar, V, Cr, Co and Ni. Our values are summarized in Table 3.5. They are based on a $3\sigma$ limit derived from the absence of strong lines in the dominant ion (usualy singly or doubly ionized) of each element in the FUSE bandpass.

## 2.7 The pattern of heavy elements in DB stars

The tally of DB white dwarfs that display photospheric carbon features now reaches 8. This allows us to get a clearer picture of the abundance pattern of that important element. Figure 3.16 presents the current observed carbon abundances in DB and DQ stars. In that figure, we combine the carbon abundances determined in this contribution, the results of

Provencal et al. (2000) for the hot DB stars GD 358 and PG 0112+104, the three objects analyzed by Petitclerc et al. (2005) as well as the upper limits in the DB white dwarfs of Wegner & Nelan (1987) as reanalyzed by Petitclerc et al. (2005), and the DQ stars of Dufour et al. (2005).

The problem of the origin of carbon in DB white dwarfs has been reviewed in some detail by Petitclerc et al. (2005), who considered the three traditional mechanisms to account for the presence of that element: radiative element support, convective dredge-up from the core and accretion from the interstellar medium. All three were argued to be inadequate in the intermediate temperature regime of the three DB stars studied, which were most likely too cool for significant radiative element support but too hot for significant dredge-up or accretion from the ISM. To account for the carbon pattern in those helium-rich degenerates, Petitclerc et al. (2005) relied on a scenario proposed by Fontaine & Brassard (2005), who suggest that the carbon observed is primordial and is left over from previous evolutionary phases that link the very hot PG 1159 stars to the DO stars and then to the DB stars. We explore this model further here, but note that Jura (2006) puts forward the alternative view that carbon in those DB white dwarfs which are characterized by low C/Fe ratios could instead be the result of accreted asteroids with a chondritic composition.

By the time a PG 1159 cools down to an effective temperature in the DB range, $T_{\rm eff} = 30,000$ K, the chemical separation of helium from carbon/oxygen is not complete, as argued by Dehner & Kawaler (1995) and Brassard & Fontaine (2003). However, in the low-density photosphere, the settling timescales are short enough for diffusion to be well advanced, and the predicted photospheric C/He ratio is a measly $10^{-15}$ (Fontaine & Brassard 2002). To prevent the complete disappearance of photospheric carbon, the idea of a weak stellar wind competing with gravitational settling has been put forward. This residual wind would be a scaled-down version of those encountered in the precursors of the DO and DB white dwarfs, the PG 1159 stars. The preliminary investigations of winds along the cooling track of Fontaine & Brassard (2005) are based on fully evolutionary models which include a linear relationship between mass loss and age, with the wind turning off completely at $T_{\rm eff} = 20,000$ K.

We show, in Figure 3.16, the photospheric carbon abundances expected on the basis of

the evolutionary models of Fontaine & Brassard (2005). Models at 0.6 $M_{\odot}$ characterized by different mass loss rates and values for the thickness of the helium envelope are shown. We note that only a single such model was available to Petitclerc et al. (2005). mass loss rates of the order of $\sim 10^{-13}$ $M_{\odot}$ $yr^{-1}$ are able to account for the observations of Petitclerc et al. (2005). The hottest star of our sample, G270-124, with its effective temperature above 20,000 K and low carbon abundance (log (C/He) $= -7.8 \pm 0.1$), can also be accomodated within this wind scenario, provided the mass loss rate is of the order of $2.5 \times 10^{-13}$ $M_{\odot}$ $yr^{-1}$, a conclusion also reached by Brassard et al. (2007) and in good agreement with the abundances determined by Petitclerc et al. (2005). For the hotter objects, above 20,000 K, the mass loss rate is the dominant parameter while the thickness of the helium envelope plays essentially no role.

In the cool DQ and DC stars, the observed carbon is believed to be intrinsic and to originate from the deeper layers of the stars and to be brought back to the photosphere by a convective dredge-up mechanism (Koester et al. 1982; Fontaine et al. 1984). As the white dwarf cools down, the tail of the carbon distribution diffuses upward from the core, while the base of the helium convection zone sinks further into the star. The ensuing carbon dredge-up brings carbon back to the photosphere of the white dwarf, which becomes increasingly contaminated until the base of the convection zone reaches a maximum depth at an effective temperature $T_{\rm eff} \sim 12,000$ K (Pelletier et al. 1986; MacDonald et al. 1998). The model has been successful at explaining the carbon observations in the realm of the DQ stars (see Dufour et al. 2005 for the latest effort). Even though the efficiency of this mechanism is expected to decrease dramatically at effective temperatures above 13,000 K, the carbon abundance we derive in the 16,700 K star GD 378 (log (C/He) $= -6.9 \pm 0.1$), appears consistent with the predictions of the dredge-up model (see Figure 3.16). The abundances predicted on the hot branch of the dredge-up peak are solely affected by the thickness of the helium envelope, as the speculative wind so effective at high effective temperatures has long died down.

On the other hand, the very low carbon abundance determined in the 15,040 K star GD 408 does not appear consistent with the predictions of the dredge-up model, as already emphasized by Chayer et al. (2007). There are at least two ways in which the low carbon abundance in

GD 408 could be reconciled with the dredge-up model. The first one is that the effective temperature of GD 408 has been significantly underestimated. To be in agreement with the dredge-up model, the surface temperature would have to be $\sim$ 18,000 K. This is unlikely, since our experiments with a higher effective temperature suggest that the surface gravity would have to be above log $g \sim 9.0$, and then our blue spectrum becomes impossible to match. The other possibility is that the thickness of the helium envelope is abnormally large. However, Figure 3.16 shows that, at that temperature, there is little residual sensitivity to the helium envelope mass. Even a thickness as large as log q(He)= $-2.0$, the maximum consistent with stellar evolution, does not improve significantly the internal consistency between observations and model predictions. A similar, although weaker, problem might be present in the hotter star GD 61 ($T_{\rm eff} = 17,340$ K), whose upper limit is at least $\sim$ 1 dex below the predicted abundance. An effective temperature of 18,200 K for this star would match the predictions of the dredge-up model but would require an exceedingly low surface gravity (log $g \sim 7.0$) and a large hydrogen abundance (log (H/He) $\sim -3.3$) to be consistent with the optical spectrum. Further FUSE observations of DB stars in the $15,000 - 20,000$ K range will help shed some light on the problems encountered on the hot side of the dredge-up model curve.

With the detection of carbon and oxygen in the photospheres of DB stars, we are also able, for the first time, to contrast the relative photospheric abundances of these two elements. Carbon is most likely dredged-up in DB stars below 20,000 K and whatever amount of oxygen is observed in these objects is also likely to have been dredged-up from the deeper layers by the same convective mechanism. Thus the observed O/C abundance ratio must be connected to the abundance profiles of these elements in the composition transition region between the nearly pure helium envelope and the He-C-O mantle, to use the terminology of Fontaine & Brassard (2002). These authors also emphasize that, even among the DB stars, the C and O settling is far from over. The only published information available at this time on the dredge-up of oxygen are the evolutionary sequences considered by MacDonald et al. (1998). While these authors put the emphasis, predictably, on the temperature range of the cooler DQ stars, some useful information can be extracted from their Figure 6. At 15,000 K, models with helium envelope masses of log q(He) $\sim -2.8$ should be characterized by log (O/He) values

between $-7.3$ and $-7.75$. For higher helium envelope masses, log q(He) $\sim -2$, the predicted values of log (O/He) are of the order of $-8.25$. A helium envelope mass of the order of log q(He) $\sim -3$ is the "optimal" choice in the realm of the DQ stars (Dufour et al. 2005) but, because the gravitational settling is ongoing in the DB range, it is likely that the "typical" helium envelope mass will be smaller for stars in the 15,000 K to 20,000 K range (Brassard & Fontaine 2003), somewhere in the log q(He) $\sim -4$ range. On the basis of the scaling observed for carbon dredge-up (see top panel of Figure 3.16), the expected oxygen abundance at 15,000 K for a helium layer of log q(He) $\sim -4$ could be $\sim 80$ higher than that observed at log q(He) $\sim -3$. Thus, we expect typical, dredge-up abundances of O in the log (O/He) range between $-5.4$ and $-5.8$. The values we determine in GD 378 and GD 61, near 17,000 K, namely log (O/He) $= -6.0$ are not inconsistent with these crude estimates.

This being said, it has not escaped our attention that the determination of O abundances in DB stars can be linked to the oxygen core mass fraction, $X_{\rm O}$, a quantity which is, in turn, related to the astrophysically important $^{12}{\rm C}(\alpha,\gamma)^{16}{\rm O}$ reaction rate. The point was already made forcefully by MacDonald et al. (1998). The possibility of constraining that rate on the basis of asteroseismological analyses of V777 Her pulsators has recently been considered by Metcalfe et al. (2001) and Metcalfe (2003), with an opposing viewpoint expressed by Fontaine & Brassard (2002). As demonstrated here, abundance determinations of oxygen in DB, as well as in the cooler DQ, stars may well provide an alternative way to get to that rate, perhaps less dependent on the details of the stellar structure.

As is the case of other heavy elements in the DBZ and the DZ stars, the silicon, iron and sulphur detected in our sample are likely to originate from external sources. Heavy elements in cool white dwarfs are generally thought to be accreted from the interstellar medium, but Alcock et al (1986) and, more recently, Jura (2006) have considered more exotic options that involve comets or tidally-destroyed asteroids. In Table 3.3, we augmented our results with the calcium abundances determined by Sion et al. (1988) for the three objects that share the DBZ classification, GD 61, GD 378 and GD 408. This allows us to compare the relative abundances in our objects (Table 3.4) with those predicted within the two-phase accretion model (Dupuis et al. 1993b). We find a general consistency, except perhaps for the Fe/Ca ratio, which is quite

large in the three objects, log (Fe/Ca) > 2.0, while the predicted value is log (Fe/Ca) < 1.2. The assumption of a solar composition in the accreting material might perhaps be at the root of this systematic trend. If such is the case, the culprit might be iron, since the Si/Ca ratios we determine appear consistent with the predictions of Dupuis et al. (1993b). Finally, we note that, in the three hotter DB stars analyzed by Petitclerc et al. (2005), the upper limits on the silicon abundance are a factor of 10 lower than the abundances we determine here. This may indicate that some mechanism, perhaps the weak residual wind proposed by Fontaine & Brassard (2005) or the more intense radiation field, inhibits accretion onto the hotter stars.

## 2.8 Concluding remarks

Our FUSE spectra reveal the presence of several transitions associated with C, O, Si, Fe and S in the photospheres of five cool helium-rich white dwarfs with effective temperatures below $T_{\rm eff} = 21,000$ K. We derive photospheric abundances for these elements, and place upper limits on the abundance of several other heavy elements of interest. We discuss existing scenarios to account for the abundance pattern of carbon in DB stars and suggest that the model of Fontaine & Brassard (2005), which includes gravitational settling and stellar wind, provides a reasonable framework to account for the carbon abundances observed in stars above 19,000 K. At lower temperatures, carbon is thought to be dredged-up from the core, and our data represent the first serious test of the dredge-up model in the 13,000−19,000 K range. With four stars in that temperature regime, the results are mixed, and there is a strong suggestion that the observed carbon abundances in cool DB stars are lower than expected on the basis of the dredge-up model. Furthermore, the oxygen abundances we determine appear consistent with that element having been dredged-up from the deeper envelope as well. Additional observations of stars that map this important region where the transition from a regime dominated by wind-driven mass loss and gravitational settling to one where dredge-up, accretion from interstellar (and circumstellar) matter and gravitational settling control the photospheric abundance of heavy elements are already planned. These will help shed light on this intriguing phase of the spectral evolution of DB stars.

## 2.9 Acknowledgements

We are grateful to P. Bergeron and J. Liebert for their help in securing blue optical data at the Steward Observatory and to R. A. Saffer for his contribution in securing red optical observations at the Kitt Peak National Observatory. This work was supported in part by the NSERC Canada and by the FQRNT (Québec).

# *Chapitre* 3

# Tableaux et Figures

TABLEAU 3.1 – Log of FUSE Observations

| Name | Program ID | Date | Aperture | MODE | Number of Exposures | Exposure Time (s) |
|---|---|---|---|---|---|---|
| GD 378 | D1680101 | 2004 May 22 | LWRS | TTAG | 14 | 18805 |
| | D1680102 | 2004 May 22 | LWRS | TTAG | 6 | 8566 |
| GD 61 | D1680201 | 2003 Oct 2 | LWRS | TTAG | 20 | 34245 |
| GD 233 | D1680301 | 2004 May 31 | LWRS | TTAG | 26 | 34608 |
| G270-124 | M1020301 | 2004 July 9 | LWRS | TTAG | 8 | 9758 |
| | M1020302 | 2004 December 19 | LWRS | TTAG | 8 | 5028 |
| GD 408 | G0620101 | 2006 August 29 | LWRS | TTAG | 11 | XXXX |

TABLEAU 3.2 – Transitions of heavy elements of photospheric origin observed in cool DB white dwarfs (Cross X indicates a detection)

| Ion | Wavelength (Å) | G270-124 | GD 233 | GD 61 | GD 378 | GD 408 |
|---|---|---|---|---|---|---|
| C II | λ1010 | | | | X | |
| C II | λ1036 | X | | | X | X |
| O I | λ989 | | | | X | |
| O I | λ999 | | | X | X | |
| O I | λ1040 | | | X | X | |
| O I | λ1152 | | | X | X | |
| Si II | λ992 | X | | X | X | X |
| Si III | λ1113 | X | | X | X | |
| Fe II | λ990 | | | | X | |
| Fe II | λ1063 | | | | X | |
| Fe II | λ1096 | | | | X | |
| Fe III | λ1122 | X | | | X | |
| Fe II | λ1125 | | | | X | |
| Fe II | λ1145 | | | X | X | X |
| S II | λ1014 | | | | X | |
| S II | λ1125 | | | | X | |

TABLEAU 3.3 – Abundances in Cool DB White Dwarfs

| | log[N(X)/N(He)] | | | | |
|---|---|---|---|---|---|
| | G270-124 | GD 233 | GD 61 | GD 378 | GD 408 |
| $T_{\rm eff}$ (K) | 20,800 | 18,410 | 17,340 | 16,700 | 15,040 |
| C | −7.8 | <−8.9 | <−8.8 | −6.9 | −8.7 |
| O | <−5.9 | <−6.2 | −6.0 | −6.0 | <−6.6 |
| Si | −7.6 | <−8.0 | −6.7 | −7.2 | −8.0 |
| Fe | −7.2 | <−7.8 | −7.6 | −7.3 | −8.0 |
| S | <−8.0 | <−8.0 | <−7.9 | −7.7 | <−8.0 |
| Ca[1] | – | – | −10 | −10 | −10 |

REFERENCE. – (1) Sion et al. (1988)

TABLEAU 3.4 – Relative abundances in Cool DB White Dwarfs

| | Solar[1] | Meteorites (C1 chondrites)[1] | G270-124 | GD 61 | GD 378 | GD 408 |
|---|---|---|---|---|---|---|
| O/C | 1.86 | 9.77 | <79 | >631 | 7.9 | <126 |
| log (C/Si) | 0.88 | −0.11 | −0.2 | <−2.1 | 0.3 | −0.7 |
| log (C/Fe) | 0.94 | −0.05 | −0.6 | <−1.2 | 0.4 | −0.7 |
| log (C/S) | 1.25 | 0.24 | >0.2 | – | 0.8 | >−0.7 |
| log (Si/Ca) | 1.20 | 1.22 | – | 3.3 | 2.8 | 2.0 |
| log (Fe/Ca) | 1.14 | 1.16 | – | 2.4 | 2.7 | 2.0 |
| log (Si/Fe) | 0.06 | 0.06 | −0.4 | 0.9 | 0.1 | 0.0 |

REFERENCE. – (1) Asplund et al. (2005)

TABLEAU 3.5 – Upper limits on the abundances of heavy elements

| | log[N(X)/N(He)] | | | | |
|---|---|---|---|---|---|
| | G270-124 | GD 233 | GD 61 | GD 378 | GD 408 |
| N | <−7.0 | <−7.6 | <−7.0 | <−7.5 | <−8.0 |
| P | <−8.7 | <−9.0 | <−8.5 | <−8.8 | <−8.8 |
| Cl | <−7.9 | <−7.5 | <−7.5 | <−7.7 | <−8.1 |
| Ar | <−8.3 | <−7.9 | <−8.0 | <−8.3 | <−8.6 |
| V | <−7.7 | <−8.0 | <−8.0 | <−8.0 | <−8.1 |
| Cr | <−7.7 | <−7.8 | <−7.8 | <−7.8 | <−7.7 |
| Co | <−7.0 | <−7.0 | <−7.0 | <−7.3 | <−7.3 |
| Ni | <−7.0 | <−7.3 | <−7.4 | <−7.5 | <−8.1 |

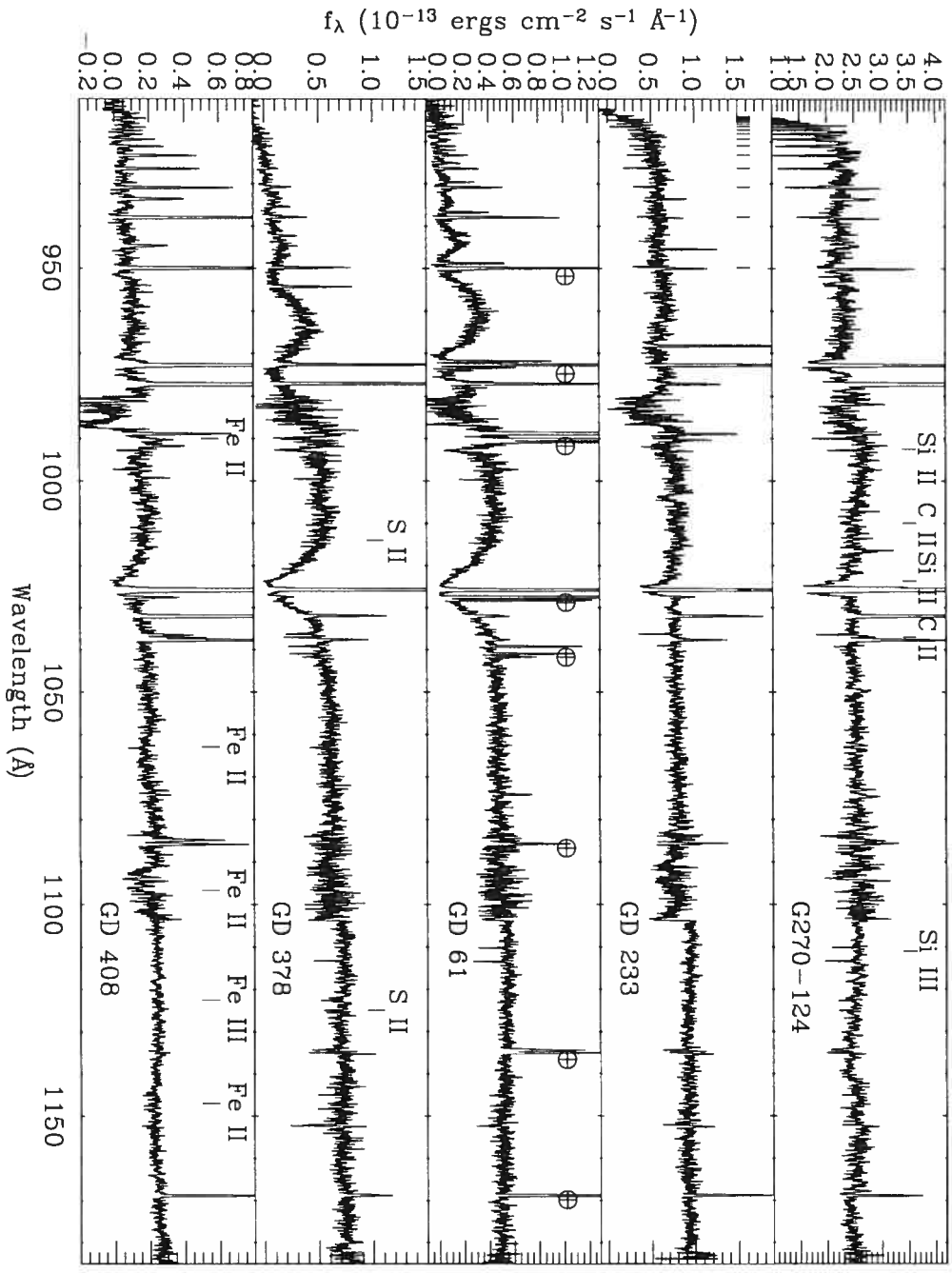


FIGURE 3.1 – Smoothed FUSE spectra of our five targets. In the top panel, the carbon and silicon lines identified in this investigation are labelled. In the second panel from the top, the location of the Lyman lines is marked. In the middle panel, the location of the strongest geocoronal emission lines is indicated with the usual symbol. In the fourth panel from the top, the S II lines observed in GD 378 are marked. In the bottom panel, the observed iron lines are labelled. The G270-124 and GD 408 spectra are smoothed with a 15-point and a 12-point average, respectively, and those of GD 233, GD 61 and GD 378 with a 18-point average.

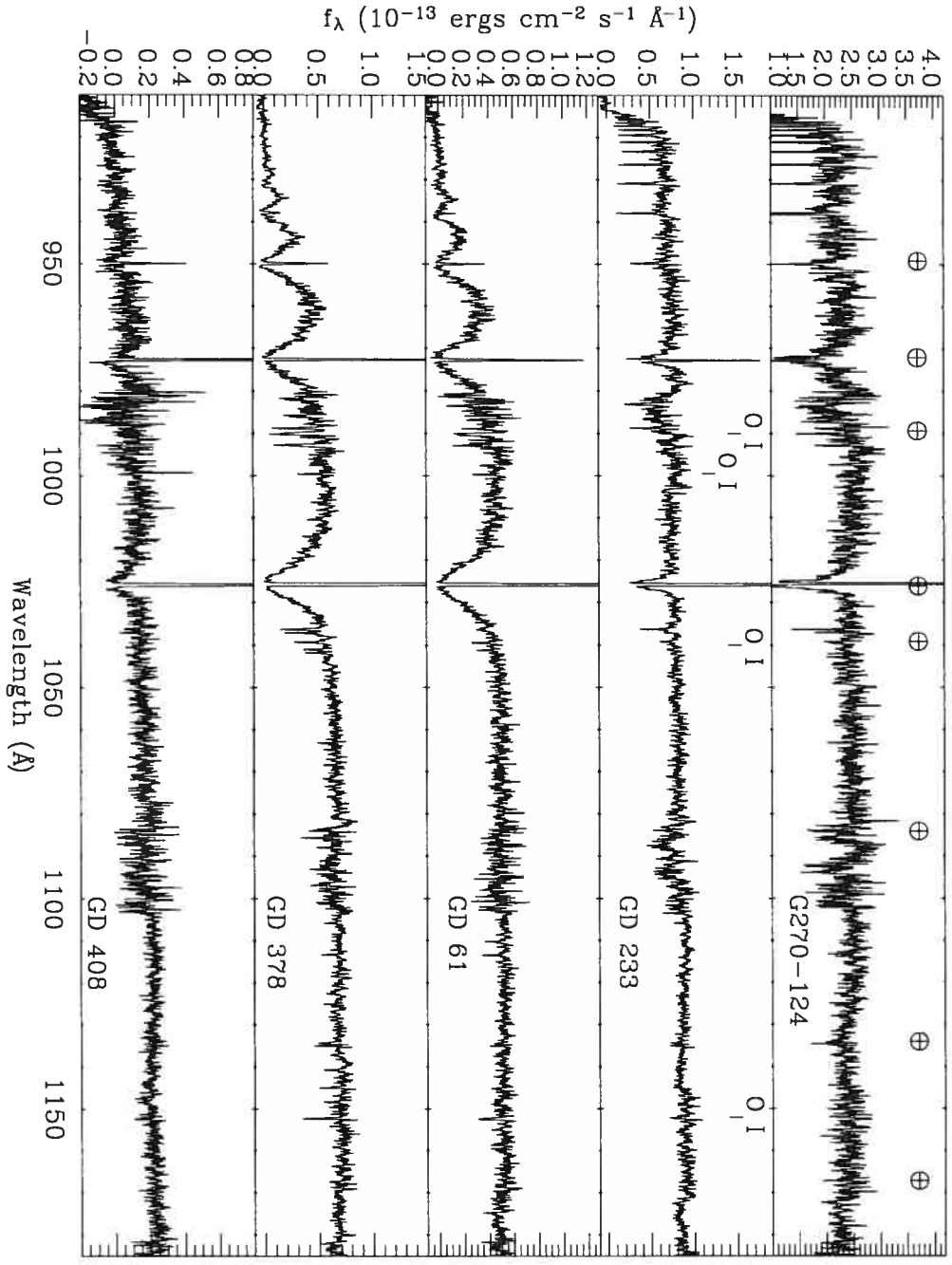


FIGURE 3.2 – Smoothed FUSE night-time data of our five stars. In the top panel, the location of geocoronal emission lines that usually contaminate the data is indicated with the usual symbol. In the second panel from the top, the photospheric oxygen lines now free from geocoronal contamination, are labelled. The G270-124 and GD 408 spectra are smoothed with a 15-point and a 12-point average, respectively, and those of GD 233, GD 61 and GD 378 with a 18-point average.

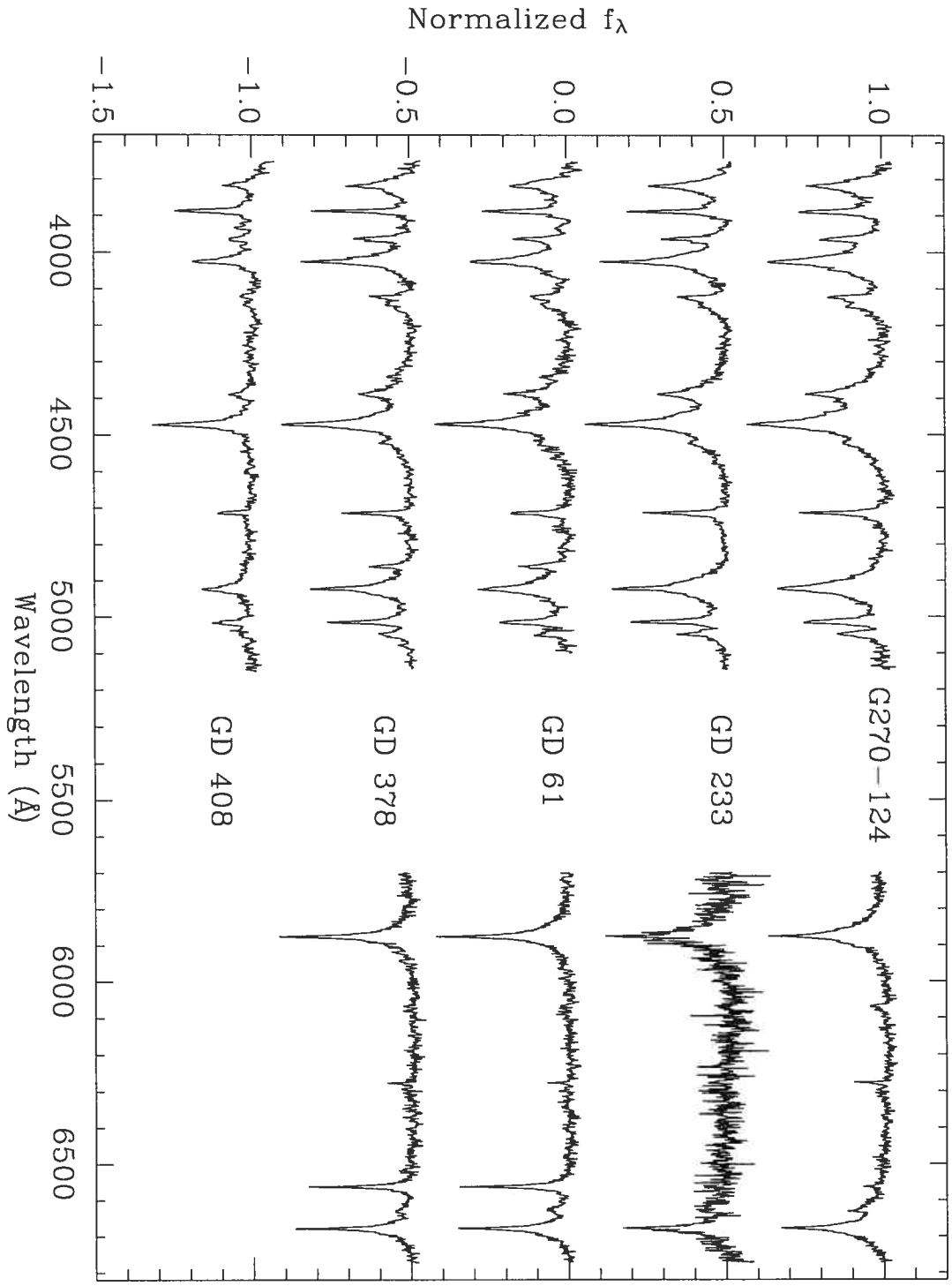


FIGURE 3.3 – Blue and red spectra of our five target stars, in order of decreasing temperature from the top. For GD 408, only blue data were available. The spectrum at the top is rectified in order to normalize the continuum to 1, while the others are rectified and each offset by 0.5.

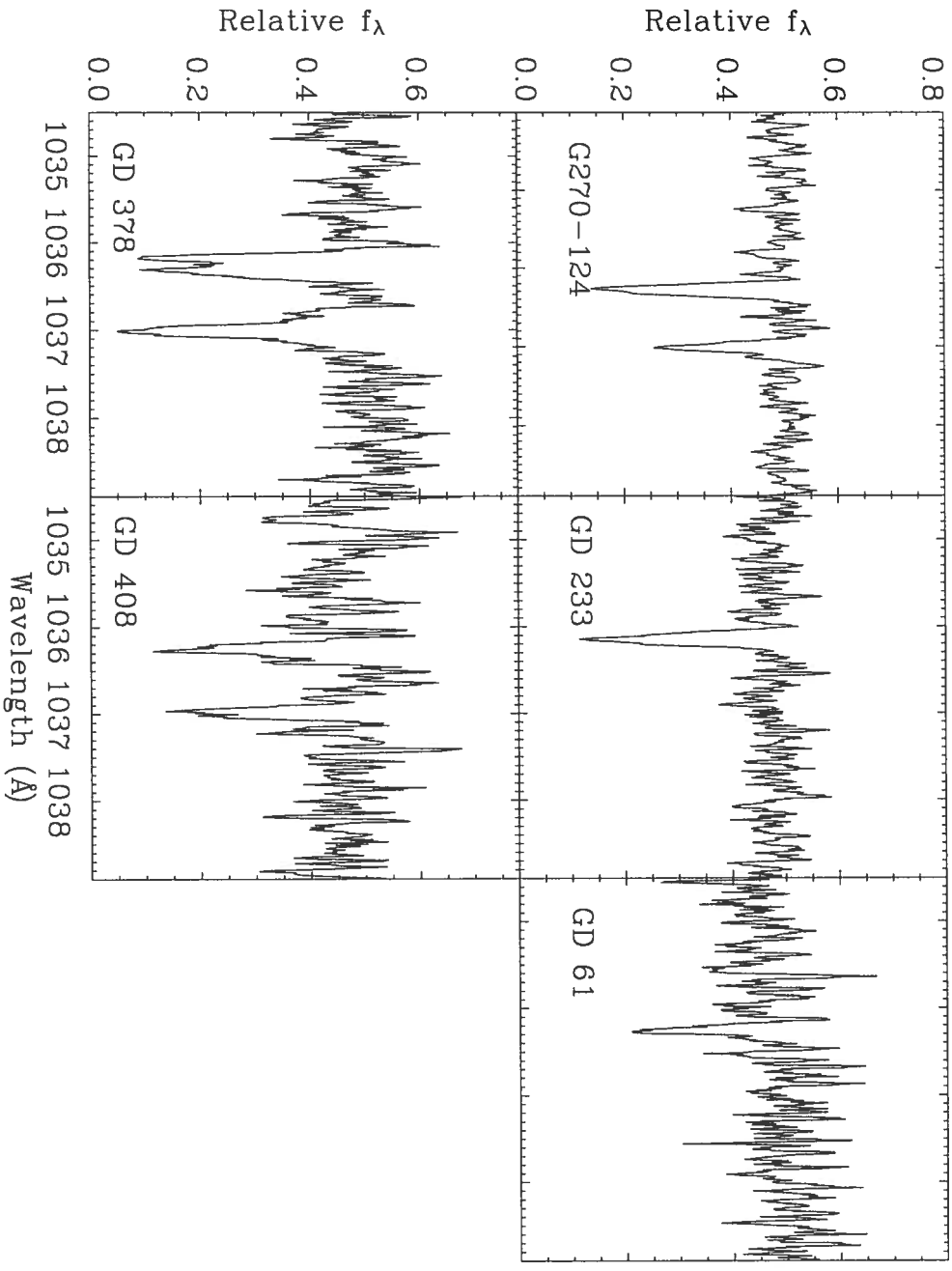


FIGURE 3.4 – The region around the resonance doublet C II $\lambda$1036.337, $\lambda$1037.018 for our five stars. G270-124, GD 378 and GD 408 show photospheric carbon. An interstellar contribution is present, especially in $\lambda$1036.337, which originates on the ground state. The feature $\lambda$1037.018 has a weaker interstellar component and originates on a level 63.4 $cm^{-1}$ above the ground state. In GD 61 and GD 233, $\lambda$1036.337 is likely to be of ISM origin only. The G270-124 spectrum is smoothed by a 2-point average, the GD 233 and GD 61 spectra by a 4-point average, the GD 378 spectrum by a 5-point average and the GD 408 spectrum by a 3-point average.

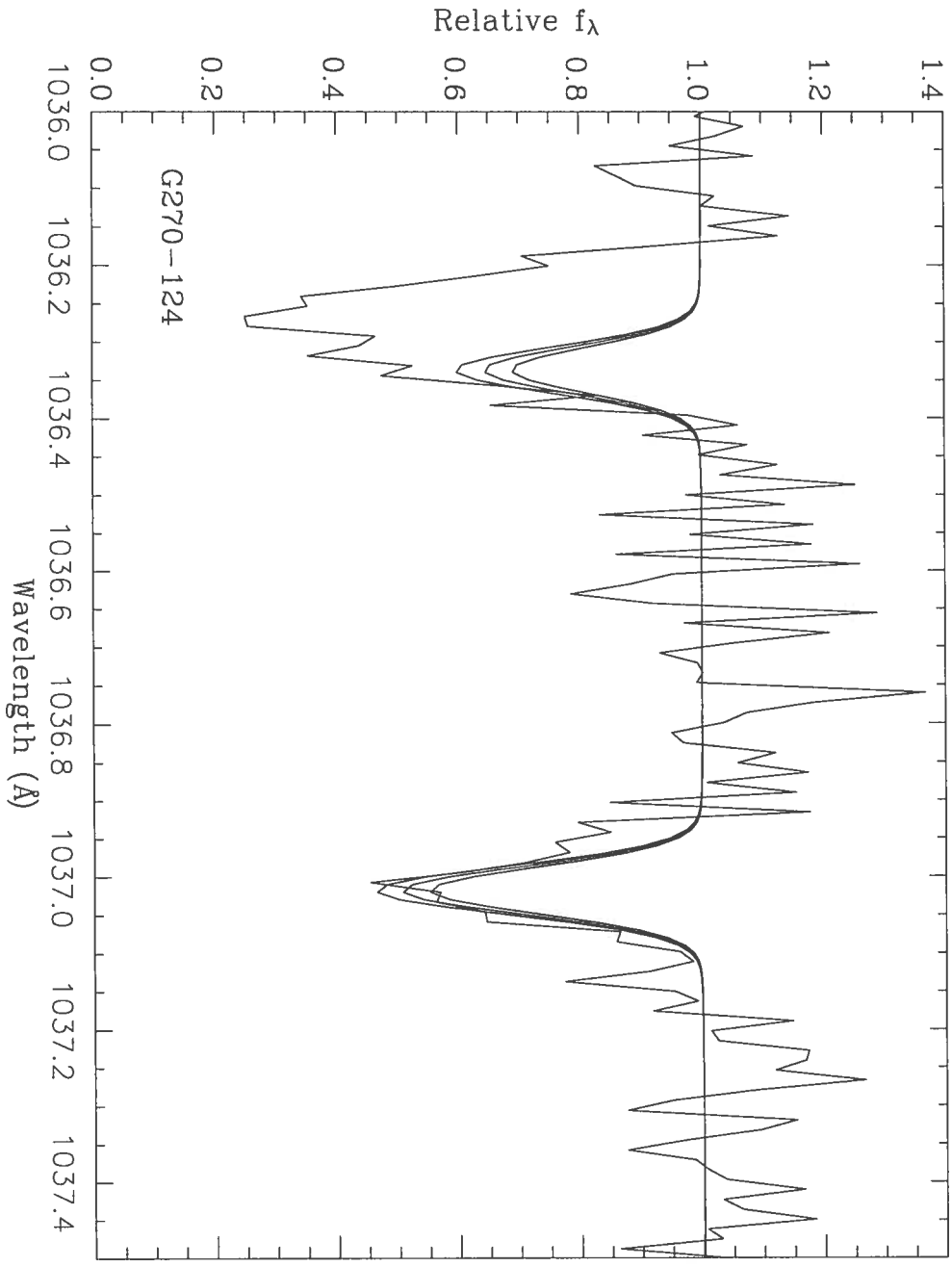


FIGURE 3.5 – Fits to the carbon feature detected in the FUSE spectrum of G270-124. An interstellar contribution is present, especially in λ1036.337, which originates from the ground state. The feature λ1037.018 has a weaker interstellar component and originates from a level 63.4 $cm^{-1}$ above the ground state. The synthetic spectra are for abundances of log (C/He) of −7.9, −7.8 and −7.7 from top to bottom.

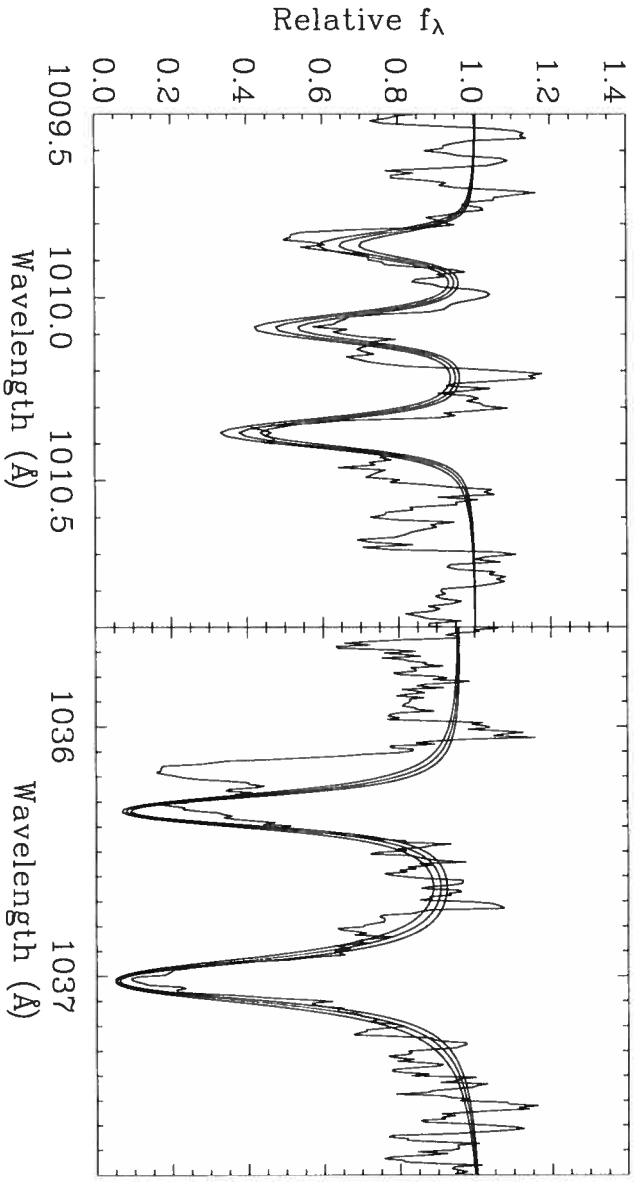


FIGURE 3.6 – Fits to the carbon features detected in the FUSE spectrum of GD 378. The synthetic spectra are for abundances of log (C/He) of −7.0, −6.9 and −6.8 from top to bottom. Observations are smoothed by a 4-point average.

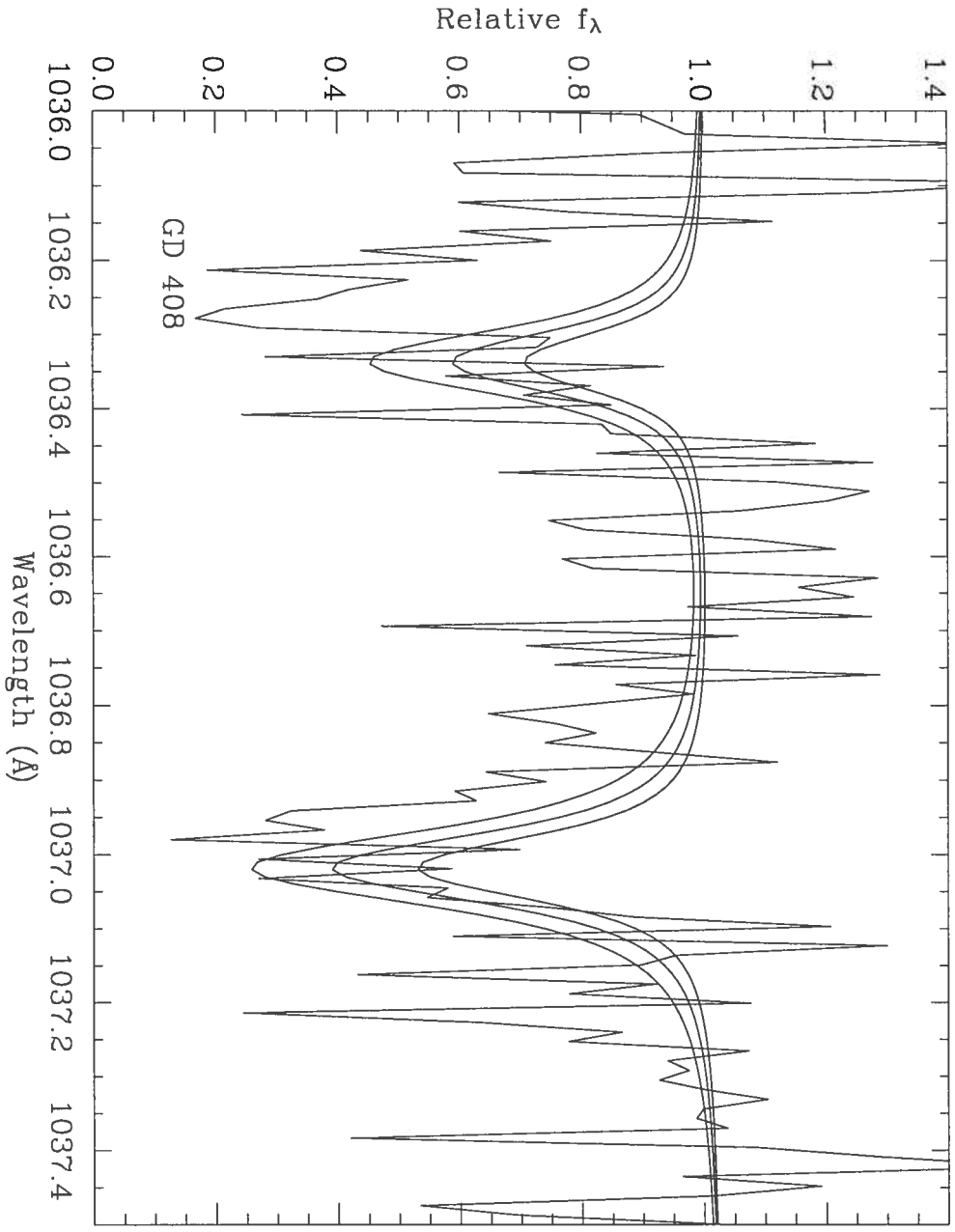


FIGURE 3.7 – Fits to the weak carbon feature detected in the FUSE spectrum of GD 408. An interstellar contribution is present in both lines. The synthetic spectra are for abundances of log (C/He) of −8.9, −8.7 and −8.5 from top to bottom.

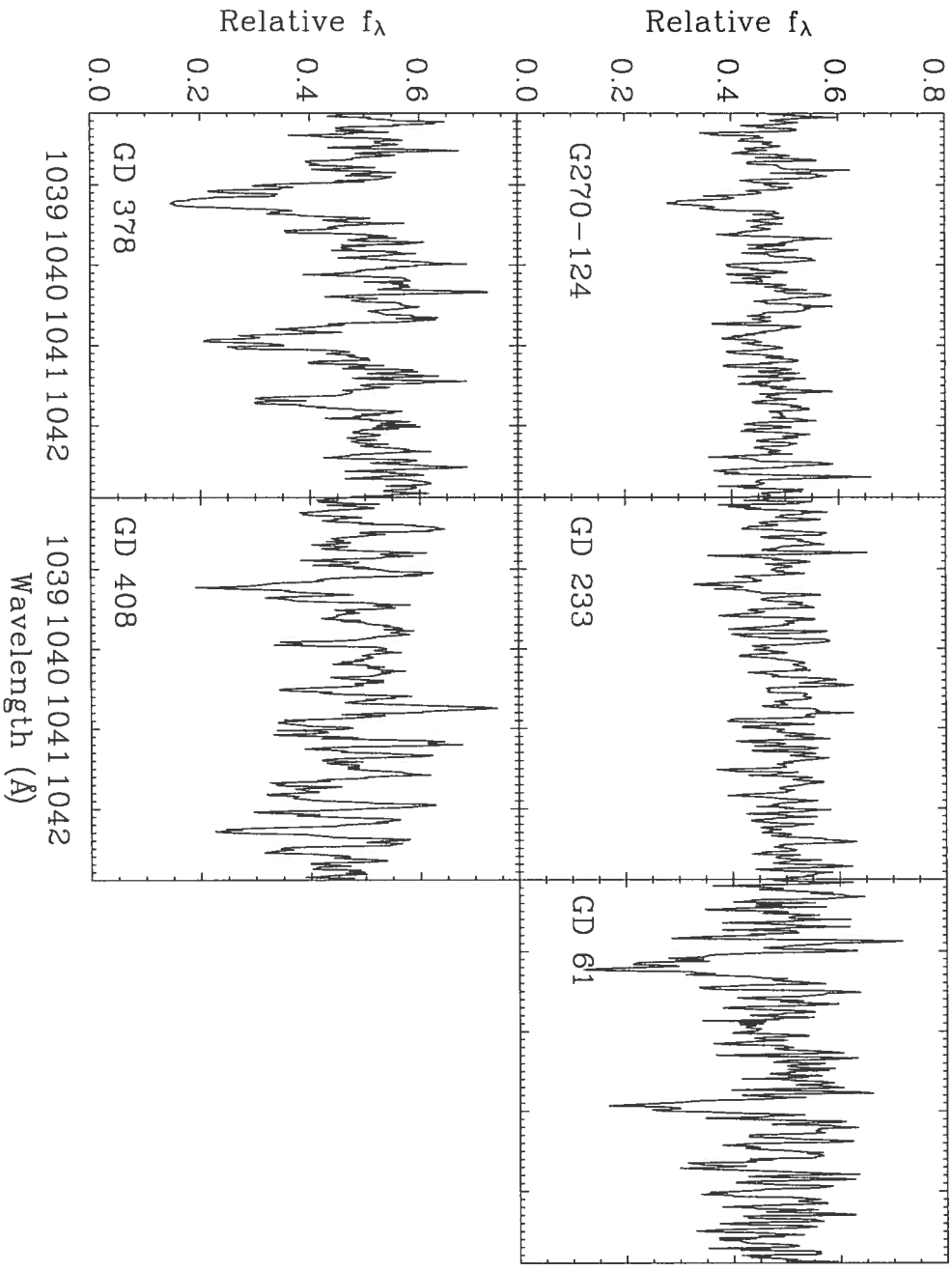


FIGURE 3.8 – The region around the triplet O I λ1039.230, λ1040.943, λ1041.688 in night-time data of the five stars. Only GD 61 and GD 378 display photospheric oxygen. An interstellar contribution is present, especially in λ1039.230 which originates on the ground state. The λ1040.943 and λ1041.688 components have a weaker interstellar contribution and originate on levels 158.265 $cm^{-1}$ and 226.977 $cm^{-1}$ above the ground state respectively. In G270-124, GD 233 and GD 408, λ1039.230 is likely to be of ISM origin only. Night-time observations of GD 408 are smoothed by a 6-point average and those of G270-124, GD 233, GD 61 and GD 378 are smoothed by a 2-point average.

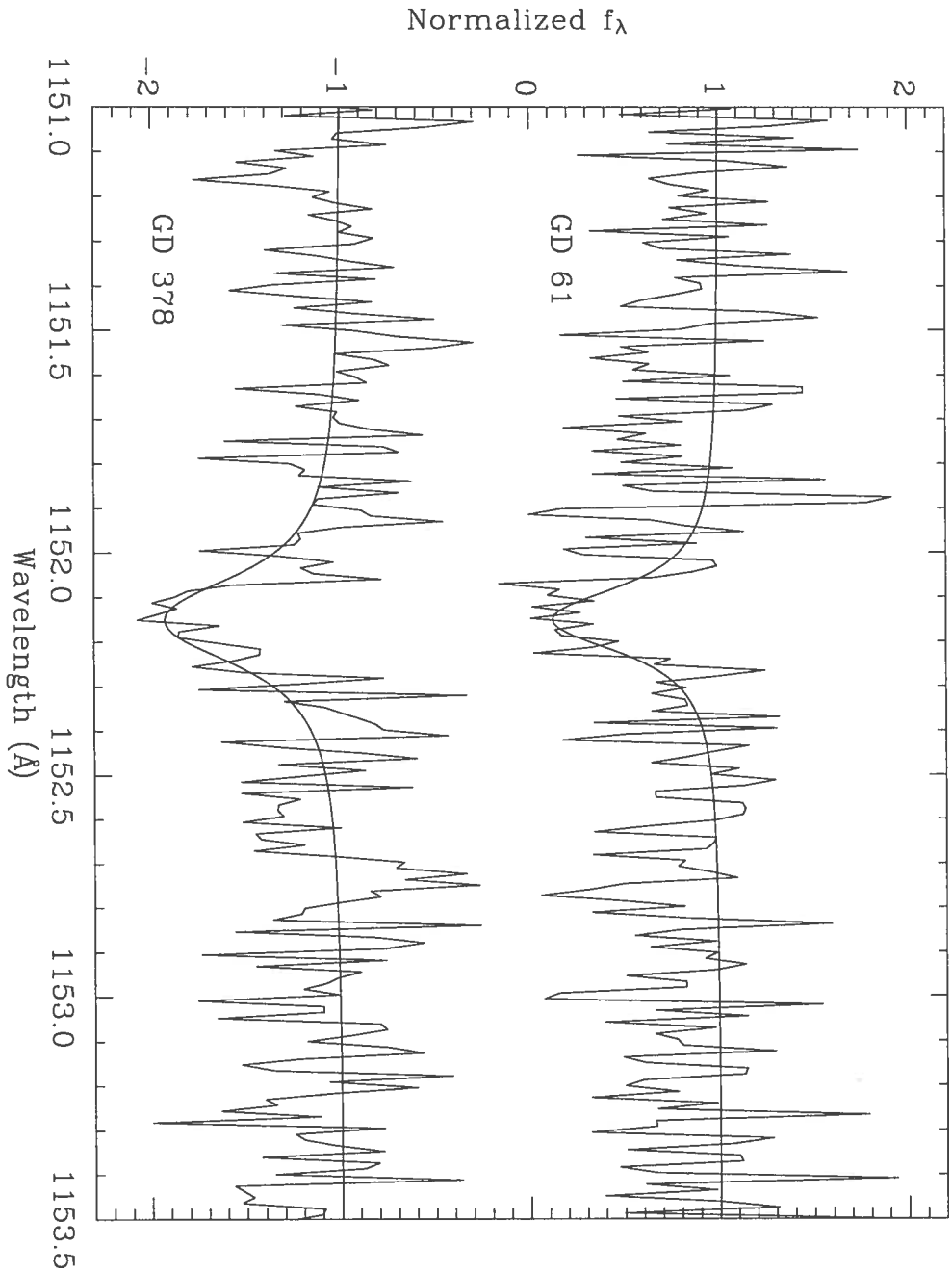


FIGURE 3.9 – Fits to the O I line λ1152.151. In addition to the O I λ1040 transition, the λ1152.151 line is observed in the night-time spectra of GD 61 and GD 378. This line is of photospheric origin, since it originates on a lower level 15,857.862 cm $^{-1}$ above the ground state. We determine an abundance of log (O/He) = −6.0 in both GD 61 and GD 378. The spectrum of GD 61 is normalized to unity and the observations of GD 378 are offset by 2.

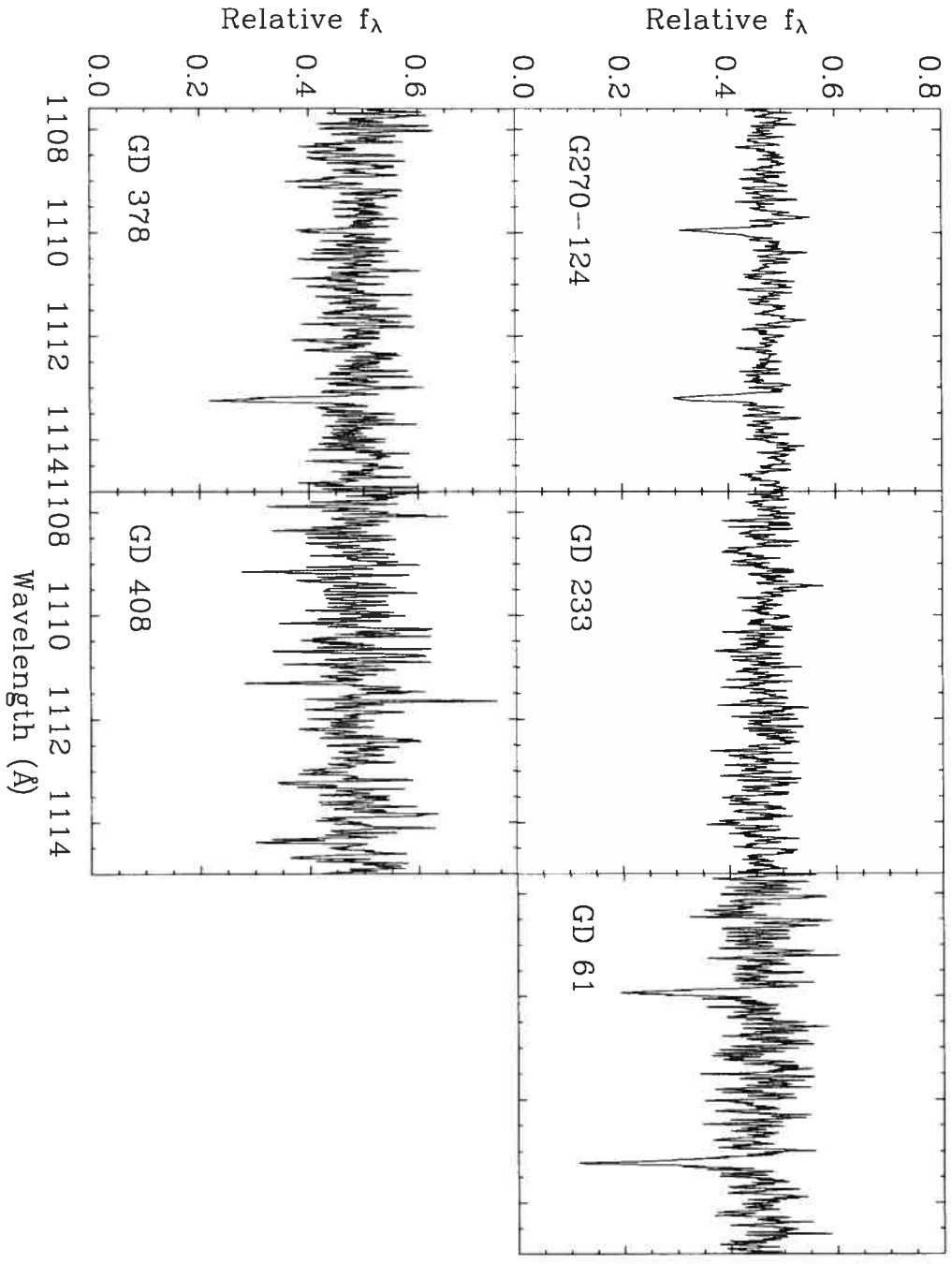


FIGURE 3.10 – The region around the Si III complex $\lambda$1108.358, $\lambda$1109.970, $\lambda$1113.204. These transitions are absent in GD 233 and GD 408, but are present in G270-124, GD 61 and GD 378 and must be of photospheric origin since they originate on a level $\sim$ 53,000 cm$^{-1}$ above the ground state. The G270-124 and GD 408 spectra are smoothed by a 2-point average, the GD 233 spectrum with a 4-point average and the GD 61 and GD 378 spectra with a 5-point average.

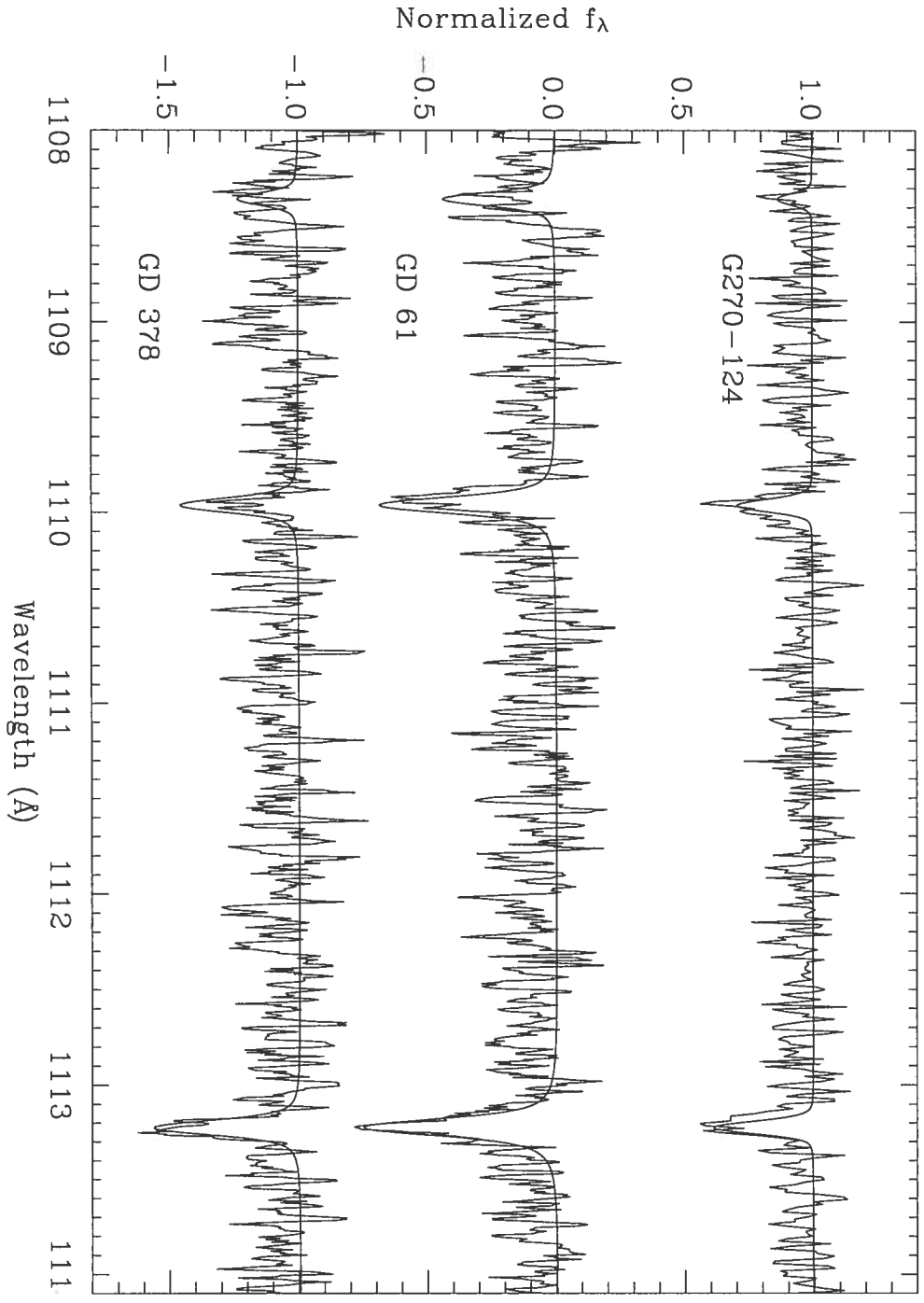


FIGURE 3.11 – Fits to the resonance triplet Si III λ1108.358, λ1109.970, λ1113.204. We determine an abundance of log (Si/He) = −7.6 in G270-124, log (Si/He) = −6.7 in GD 61 and log (Si/He) = −7.2 in GD 378. The GD 61 and GD 378 spectra are smoothed with a 2-point average. The spectrum of G270-124 is normalized to unity, while the others are offset by one unit.

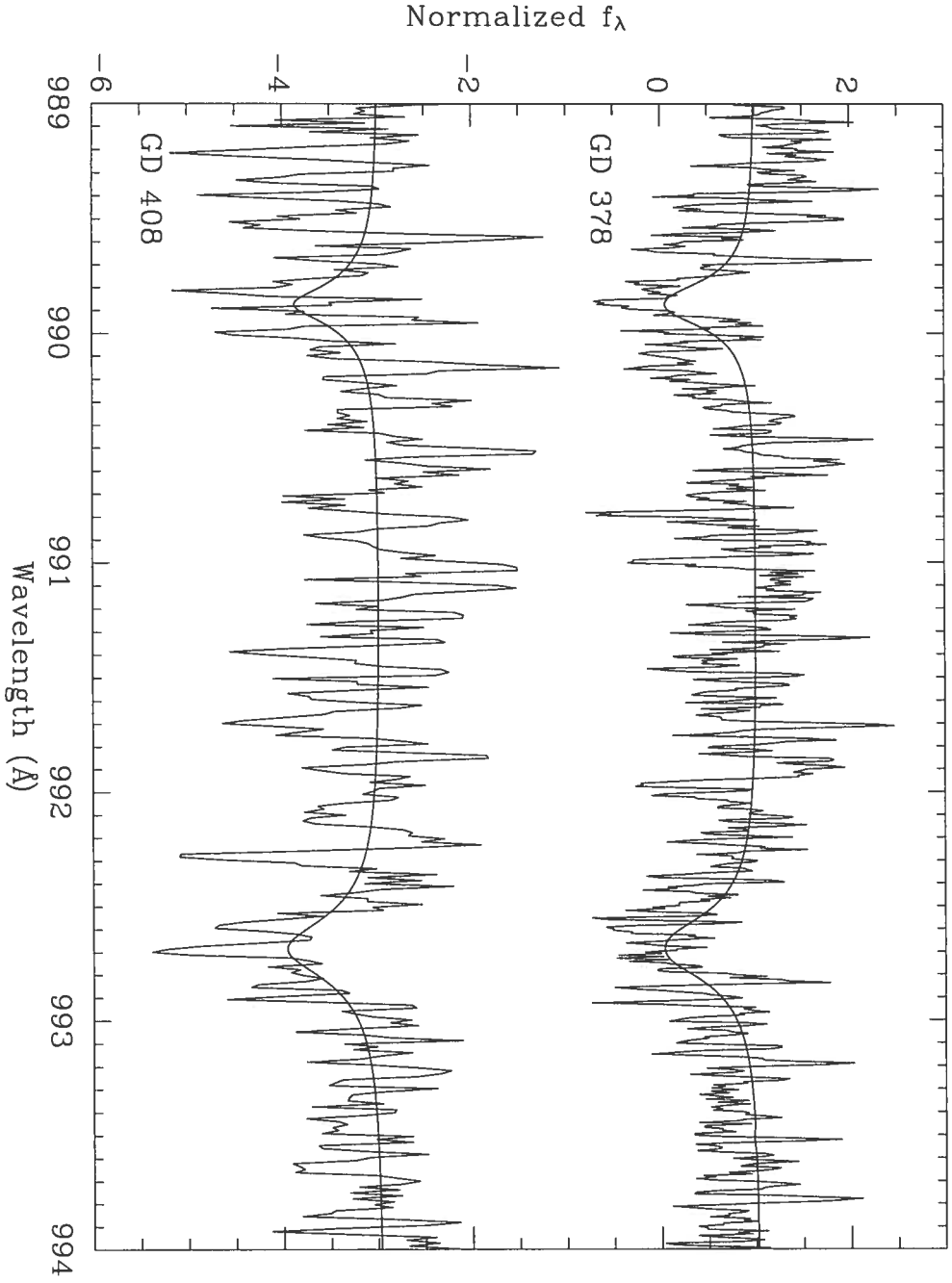


FIGURE 3.12 – Fits to the Si II complex $\lambda$989.873, $\lambda$992.683, $\lambda$992.696. The coolest target, GD 408, does not display the Si III feature $\lambda$1113, but its spectrum shows transitions associated with Si II. From Si II, we determine an abundance of log (Si/He) = −8.0 in that star. The spectrum is compared to that of the hotter star GD 378, whose abundance is based mostly on Si III transitions. Observations are smoothed by a 2-point average and spectrum of GD 408 is offset by four units.

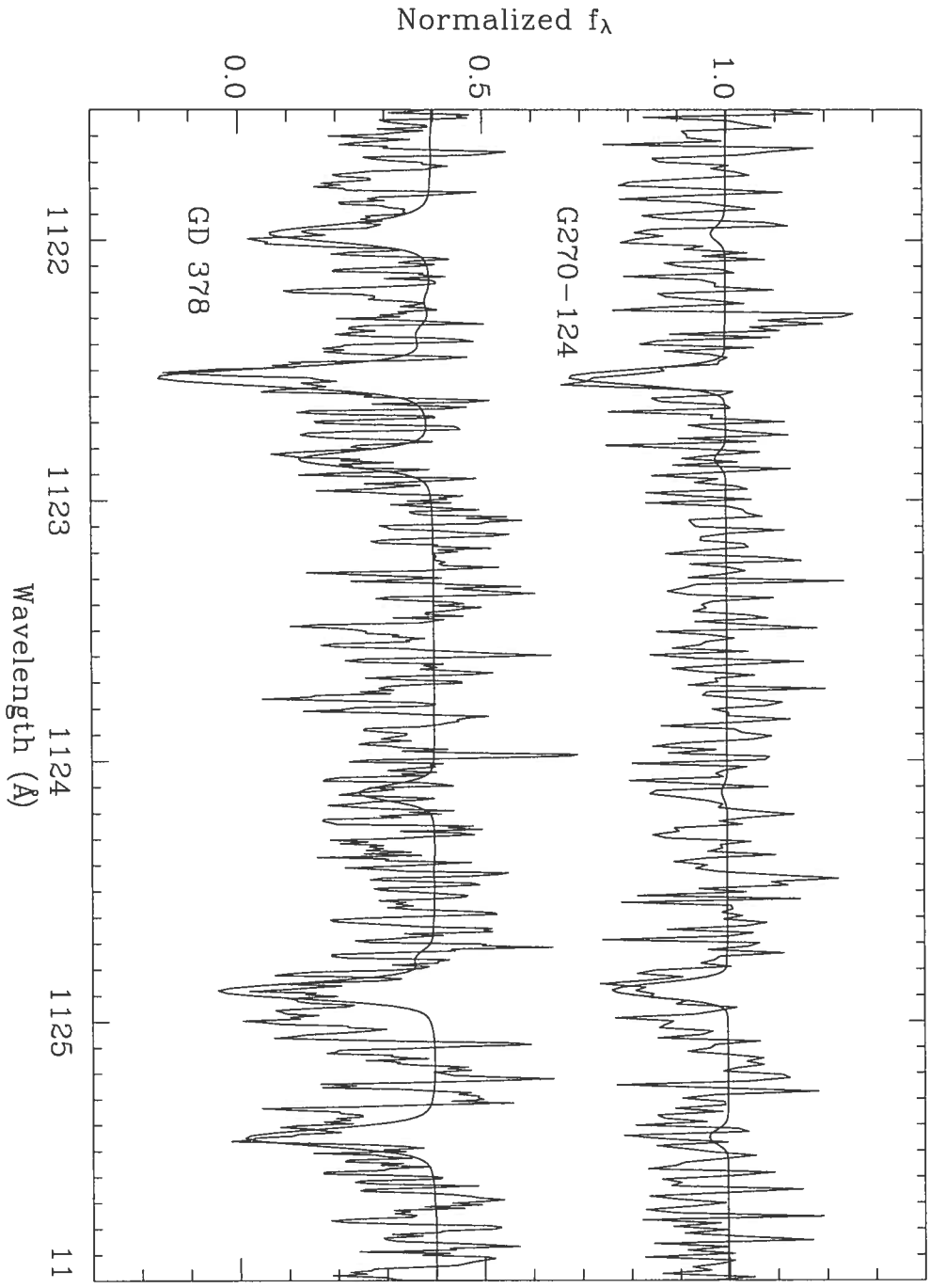


FIGURE 3.13 – Fits to Fe II and Fe III transitions. The spectrum of hottest target, G270-124, displays only photospheric transitions associated with the Fe III ion. The component $\lambda$1122.526 originates on the ground state but $\lambda$1124.881 originates on an excited level 436.2 $cm^{-1}$ above the ground state. GD 378 also shows this doublet along with several other Fe II transitions. We derive an abundance of log (Fe/He) = −7.2 in G270-124 and log (Fe/He) = −7.3 in GD 378. The spectrum of G270-124 is normalized to unity, and the observations of GD 378 are smoothed with a 3-point average and offset by 0.6.

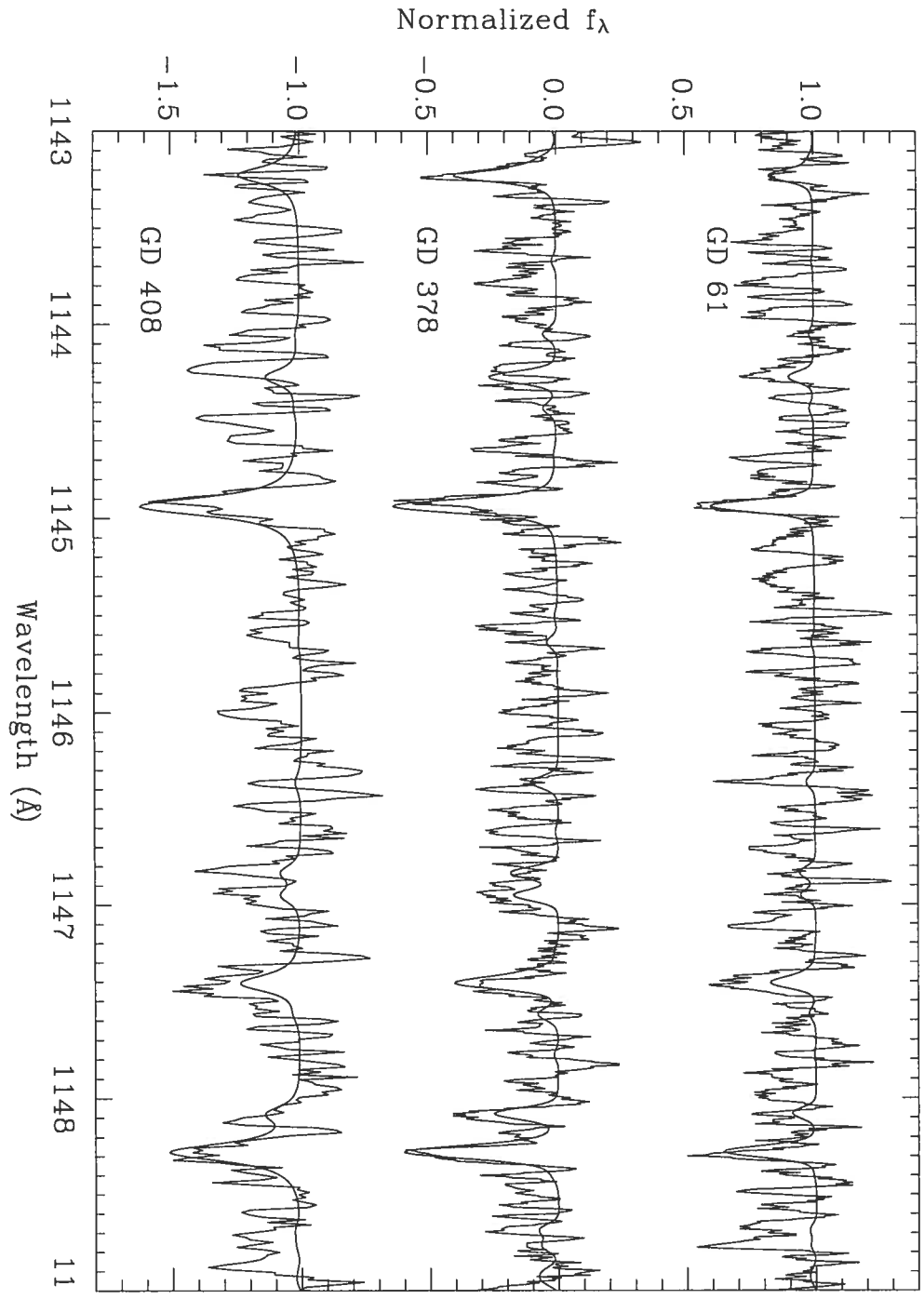


FIGURE 3.14 – Fits to Fe II transitions. The λ1145 complex is observed in the three coolest targets. An interstellar component is present in λ1144.938, which originates from the ground state. The λ1147.409 and λ1148.277 lines originate from a lower level 384.79 cm $^{-1}$ above the ground state and are of photospheric origin. We determine an abundance of log (Fe/He) = −7.6 in GD 61, log (Fe/He) = −7.3 in GD 378 and log (Fe/He) = −8.0 in GD 408. The GD 61 and GD 378 spectra are smoothed with a 5-point average while the spectrum of GD 408 is smoothed by a 2-point average. The observations of GD 61 are normalized to unity while the other spectra are offset by one unit.

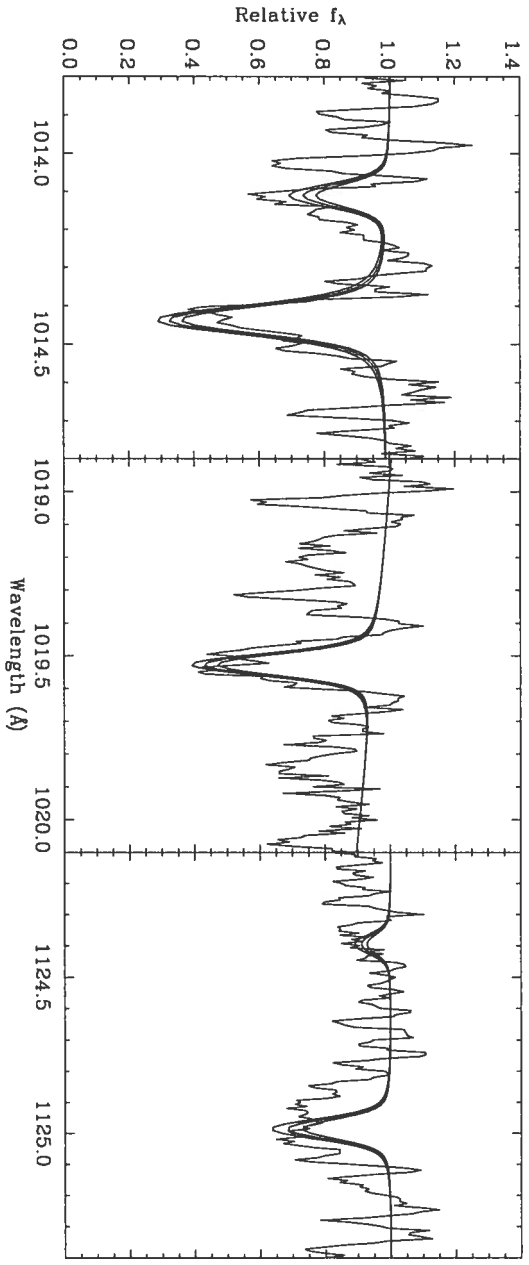


FIGURE 3.15 – Fits to the photospheric sulphur features detected in the FUSE spectrum of GD 378. The complex at $\lambda$1014 originate from lower levels $> 14,800$ cm$^{-1}$ above the ground state while the line $\lambda$1124.986 has its lower level 24,571.54 cm $^{-1}$ above the ground state. The synthetic spectra are for abundances of log (S/He) of $-7.8$, $-7.7$ and $-7.6$ from top to bottom. Observations are smoothed with a 4-point average.

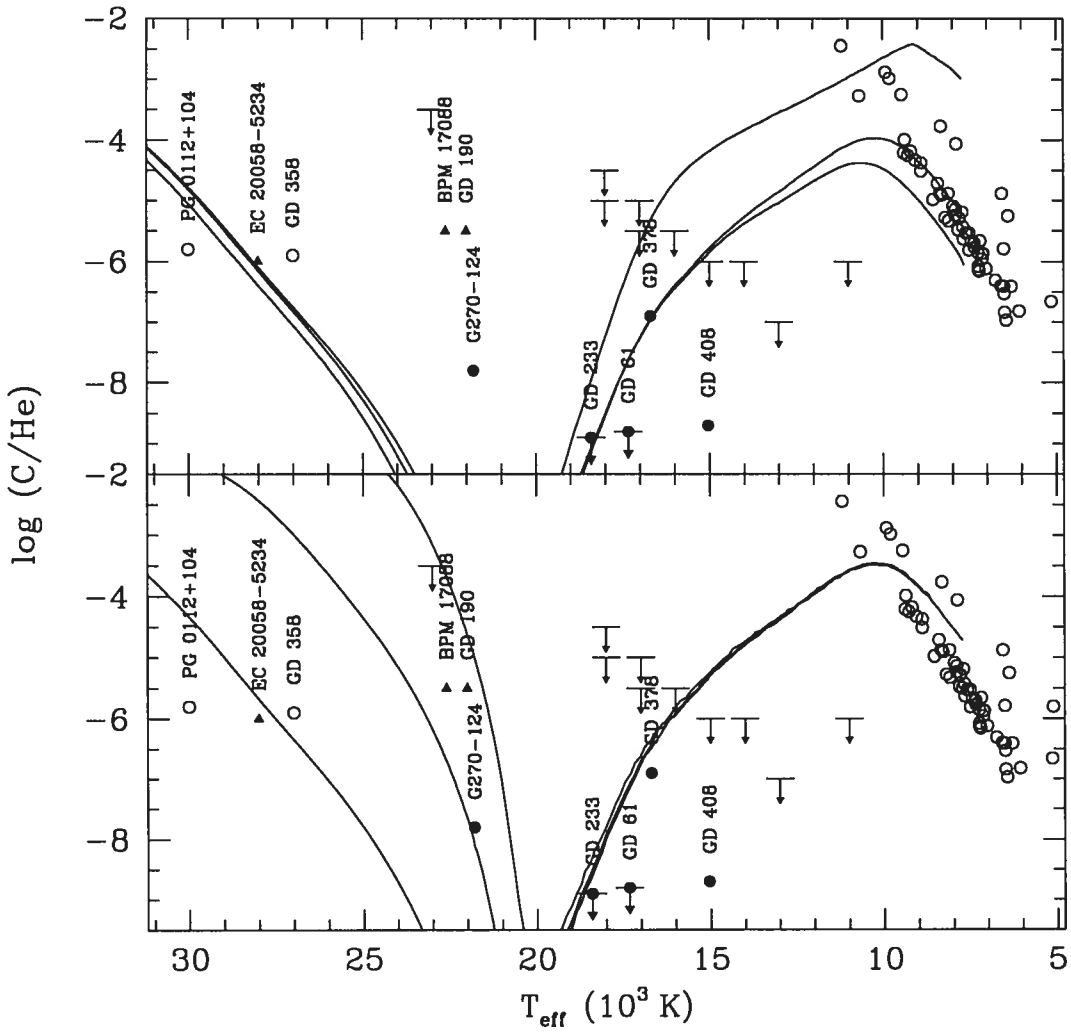


FIGURE 3.16 – Observed carbon abundances in helium-rich white dwarfs. At the hot end, we include the results of Provencal et al. (2000) (open circles), as well as the three objects analyzed by Petitclerc et al. (2005) (filled triangles). The five stars analyzed here are identified with filled circles and arrows (upper limits in GD 233 and GD 61). The upper limits in the DB stars of Wegner & Nelan (1987), as reanalyzed by Petitclerc et al. (2005), are shown with simple arrows. At cooler temperatures, the DQ stars analyzed by Dufour et al. (2005) are shown as open circles. The solid lines are evolutionary models of Fontaine & Brassard (2005) showing the expected photospheric carbon abundance distributions for a 0.6 $M_\odot$ star. The top panel shows the expected distribution for thicknesses of the helium convection zone of, from top to bottom, log q(He) = −4.0, −3.0, and −2.0. The bottom panel shows the expected distribution for mass loss rates of, from bottom to top, '1 X', '2.5 X' and '5.0 X' $10^{-13}$ $M_\odot$. Above 23,000 K, mass loss and diffusion are the dominant mechanisms. Below 19,000 K, the "windy" past of cool helium-rich degenerates does not affect the dredge-up mechanism that brings carbon back to the stellar surface.

*Chapitre* 4

# Conclusion

Dans le cadre de cette étude, nous avons d'abord redéterminé les paramètres atmosphériques de cinq naines blanches froides en utilisant une procédure de minimisation $\chi^2$, une grille de modèles étendue et améliorée par rapport à celle utilisée lors d'études antérieures ainsi que les spectres des régions bleue et rouge du visible obtenus au Steward Observatory et au Kitt Peak National Observatory. Les valeurs des paramètres fondamentaux que nous avons mesurées semblent en accord avec les déterminations antérieures disponibles dans la littérature. Seule la détermination de ces paramètres pour l'étoile la plus froide de notre échantillon, GD 408, nous semble incertaine puisque seul le spectre bleu est disponible pour cet objet. De plus, l'élargissement des raies par effet van der Waals domine pour cette étoile froide et est plus difficile à modéliser que dans le cas de l'effet Stark qui joue un rôle dominant dans les étoiles plus chaudes.

L'analyse spectroscopique dans l'ultraviolet lointain de nos objets nous a ensuite permis de contraindre ou de déterminer les abondances de cinq éléments traces. Le spectre FUSE de trois de nos objets montre la présence de carbone photosphérique. Ce résultat permet d'accroître à huit le nombre de naines blanches de type DB dont le spectre montre cet élément.

L'abondance mesurée pour l'objet le plus chaud de notre échantillon, G270−124, est évaluée à $\log\,(\mathrm{C/He}) = -7.8 \pm 0.1$. Cette valeur est un facteur $\sim 25 - 250$ plus faible que dans les étoiles plus chaudes étudiées par Petitclerc et al. (2005), mais peut quand même être expliquée dans le cadre du scénario de vent stellaire de Fontaine & Brassard (2005) avec

un taux de perte de masse d'environ $2.5 \times 10^{-13}$ $M_\odot\,yr^{-1}$. Les deux autres étoiles montrant du carbone sont, elles, les objets les plus froids. L'abondance de carbone mesurée dans GD 378 (log (C/He) $= -6.9 \pm 0.1$) est cohérente avec les prédictions du modèle de dragage convectif présent dans les étoiles froides. Cependant, l'abondance mesurée dans GD 408 (log (C/He) $= -8.7 \pm 0.2$) est en désaccord avec ce modèle. La limite supérieure estimée dans GD 61 représente également un problème. Pour faire disparaître l'incohérence entre les observations et les prédictions, la température effective de ces deux objets devrait être supérieure de plusieurs milliers de K à la valeur que nous avons déterminée. Ceci semble peu plausible, puisque de telles températures effectives ne cadreraient pas avec les spectres visibles de ces objets.

Nous avons également détecté des transitions associées à l'oxygène neutre dans deux étoiles, ce qui constitue une première pour des naines blanches de type DB. Le rapport O/C qui devient disponible avec des observations de ce type pourrait être utilisé afin de contraindre la fraction de masse $X_O$ dans le cœur de la naine blanche. Cette fraction de masse est évidemment reliée au taux de la réaction $(\alpha, \gamma)$ sur le $^{12}C$ sur la branche asymptotique des géantes. Des modèles détaillés de dragage de l'oxygène devraient être explorés afin de fournir des indications précises sur l'efficacité relative de ce processus pour le carbone et l'oxygène. De plus, des transitions associées au silicium et au fer ont été observées dans les spectres ultraviolets de quatre objets. Le soufre a aussi été détecté dans la photosphère de GD 378. De notre échantillon, une seule étoile, GD 233, ne montre la présence photosphérique d'aucun élément lourd. Le silicium, le fer et le soufre observés proviennent tous de sources externes à nos étoiles et les abondances mesurées semblent globalement cohérentes avec les prédictions du modèle en deux phases d'accrétion/diffusion à partir du milieu interstellaire de Dupuis et al. (1993b).

Cet échantillon d'objets nous a permis d'explorer de façon détaillée la fascinante région de transition entre un régime dominé par le tri gravitationnel et les vents stellaires et un régime où le dragage, l'accrétion de matière interstellaire (et circumstellaire) et le tri gravitationnel contrôlent les abondances photosphériques de carbone et d'autres éléments lourds. Pour les naines blanches de type DB, cette région se situe à des températures effectives entre 21,000 K et 18,000 K.

# *Annexe* A

# Transitions d'éléments lourds

Cette section se veut une énumération de toutes les transitions associées à des éléments lourds détectés dans les spectres FUSE des cinq naines blanches observées. Le tableau qui suit inclut la longueur d'onde (en Å) de la transition, l'atome ou ion associé, ainsi que l'énergie du niveau le plus bas (en $cm^{-1}$). Un X correspond à une raie observée tandis qu'un tiret – signifie que la raie est absente.

TABLEAU A.1 – Transitions d'éléments lourds observées dans la photosphère de naines blanches froides de type DB

| Longueur d'onde Å | Ion | $E_i$ - $E_k$ ($cm^{-1}$) | G 270−124 | GD 233 | GD 61 | GD 378 | GD 408 |
|---|---|---|---|---|---|---|---|
| *Carbone* | | | | | | | |
| 1009.858 | C II | [43003.300 - ] | – | – | – | X | – |
| 1010.083 | C II | [43025.300 - ] | – | – | – | X | – |
| 1010.371 | C II | [43053.600 - ] | – | – | – | X | – |
| 1036.337 | C II | [0.000 - ] | X | X | X | X | X |
| 1037.018 | C II | [63.420 - ] | X | – | – | X | X |
| *Oxygène* | | | | | | | |
| 988.655 | O I | [0.000 - ] | – | – | – | X | – |
| 988.773 | O I | [0.000 - ] | X | X | X | X | – |
| 990.127 | O I | [158.265 - ] | – | – | – | X | – |
| 990.204 | O I | [158.265 - ] | – | – | – | X | – |
| 990.801 | O I | [226.977 - ] | – | – | – | X | – |
| 999.497 | O I | [15867.862 - ] | – | – | X | X | – |
| 1039.230 | O I | [0.000 - ] | X | X | X | X | X |
| 1040.943 | O I | [158.265 - ] | – | – | X | X | – |
| 1041.688 | O I | [226.977 - ] | – | – | X | X | – |
| 1152.151 | O I | [15867.862 - ] | – | – | X | X | – |
| *Silicium* | | | | | | | |
| 989.873 | Si II | [0.000 - ] | X | – | X | X | X |
| 992.683 | Si II | [287.240 - ] | X | – | X | X | X |
| 992.696 | Si II | [287.240 - ] | X | – | X | X | X |
| 1020.699 | Si II | [0.000 - ] | – | X | X | X | – |
| 1023.700 | Si II | [287.240 - ] | – | – | – | – | – |
| 1108.358 | Si III | [52727.691 - ] | X | – | – | X | – |
| 1109.970 | Si III | [52853.281 - ] | X | – | X | X | – |
| 1113.204 | Si III | [53115.012 - ] | X | – | X | X | – |
| 1113.230 | Si III | [53115.012 - ] | X | – | X | X | – |

Tableau A.1 –– suite

| Longueur d'onde Å | Ion | $E_i$ - $E_k$ ($cm^{-1}$) | G 270−124 | GD 233 | GD 61 | GD 378 | GD 408 |
|---|---|---|---|---|---|---|---|
| *Fer* | | | | | | | |
| 989.895 | Fe II | [1872.567 - ] | – | – | – | X | – |
| 990.859 | Fe II | [2430.097 - ] | – | – | – | X | – |
| 1063.176 | Fe II | [0.000 - ] | – | – | – | X | X |
| 1068.346 | Fe II | [384.790 - ] | – | – | – | X | – |
| 1071.584 | Fe II | [667.683 - ] | – | – | – | X | – |
| 1075.635 | Fe II | [862.613 - ] | – | – | – | X | – |
| 1096.607 | Fe II | [384.790 - ] | – | – | – | X | – |
| 1096.877 | Fe II | [0.000 - ] | – | – | – | X | – |
| 1121.975 | Fe II | [0.000 - ] | – | – | – | X | – |
| 1122.526 | Fe III | [0.000 - ] | X | – | X | X | – |
| 1124.881 | Fe III | [436.200 - ] | X | – | – | X | – |
| 1125.448 | Fe II | [0.000 - ] | – | – | – | X | – |
| 1128.046 | Fe II | [977.053 - ] | – | – | – | X | – |
| 1143.226 | Fe II | [0.000 - ] | – | – | – | X | X |
| 1144.938 | Fe II | [0.000 - ] | – | – | X | X | X |
| 1147.409 | Fe II | [384.790 - ] | – | – | X | X | X |
| 1148.277 | Fe II | [384.790 - ] | – | – | X | X | X |
| 1151.146 | Fe II | [667.683 - ] | – | – | – | X | X |
| *Soufre* | | | | | | | |
| 1014.110 | S II | [14852.870 - ] | – | – | – | X | – |
| 1014.437 | S II | [14884.670 - ] | – | – | – | X | – |
| 1019.528 | S II | [14852.870 - ] | – | – | – | X | – |
| 1124.986 | S II | [24571.539 - ] | – | – | – | X | – |

# *Bibliographie*


Aanestad, P. A., Kenyon, S. J., Hammond, G. L., & Sion, E. M. 1993, AJ, 105, 1033

Alcock, C., Fristrom, C. C., & Siegelman, R. 1986, ApJ, 302, 462

Asplund, M., Grevesse, N., & Sauval, A. J. 2005, in ASP Conf. Ser. 336 : Cosmic Abundances as Records of Stellar Evolution and Nucleosynthesis in honor of David L. Lambert, ed. T. G. Barnes III & F. N. Bash, 25

Beauchamp, A. 1995, PhD. thesis, Université de Montréal

Beauchamp, A., Wesemael, F., Bergeron, P., Fontaine, G., Saffer, R.A., Liebert, J. & Brassard, P. 1999, ApJ, 516, 887

Bica, E., Bonatto, C., & Giovannini, O. 1996, AAS, 119, 211

Brassard, P. & Fontaine, G. 2003, in Asteroseismology Across the HR Diagram 284 : Proceedings of the Asteroseismology Workshop, ed. M. J. Thompson, M. S. Cunha, & M. J. P. F. G. Monteiro, 501

Brassard, P., Fontaine, G., Dufour, P., & Bergeron, P. 2007, in ASP Conf. Ser. : 15th European Workshop on White Dwarfs, in press

Castanheira, B. G., Kepler, S. O, Handler, G., & Koester, D. 2006, AA, 450, 331

Chayer, P., Desharnais, S., Wesemael, & Kruk, J. W. 2007, in Proceedings of American Astronomical Society Meeting 209, in press

Dehner, B. T. & Kawaler, S. D. 1995, ApJL, 445, L141

Desharnais, S., Wesemael, F., Chayer, P., & Kruk, J. W. 2007, in ASP Conf. Ser. : 15th European Workshop on White Dwarfs, in press

Dreizler, S. & Werner, K. 1996, AA, 314, 217

Dufour, P., Bergeron, P., & Fontaine, G. 2005, ApJ, 627, 404

Dufour, P., Wesemael, F., & Bergeron, P. 2002, ApJ, 575, 1025

Dupuis, J., Fontaine, G., Pelletier, C., & Wesemael, F. 1992, ApJS, 82, 505

Dupuis, J., Fontaine, G., Pelletier, C., & Wesemael, F. 1993a, ApJS, 84, 73

Dupuis, J., Fontaine, G., & Wesemael, F. 1993b, ApJS, 87, 345

Eisenstein, D. J., Liebert, J., Koester, D., Kleinmann, S. J., Nitta, A., Smith, P. S., Barentine, J. C., Brewington, H. J., Brinkmann, J., Harvanek, M., Krzesiński, J., Neilsen, Jr., E. H., Long, D., Schneider, D. P. & Snedden, S. A. 2006, AJ, 132, 676

Feldmann, P. D., Sahnow, D. J., Kruk, J. W., Murphy, E. M. Moos, & H. W. 2001, JGR, 106, 8119

Fontaine, G. & Brassard, P. 2002, ApJL, 581, L33

Fontaine, G. & Brassard, P. 2005, in ASP Conf. Ser. 334 : 14th European Workshop on White Dwarfs, ed. D. Koester & S. Moehler, 49

Fontaine, G., Villeneuve, B., Wesemael, F., & Wegner, G. 1984, ApJ, 277, L61

Fontaine, G., Villeneuve, B., & Wilson, J. 1981, ApJ, 243, 550

Fontaine, G. & Wesemael, F. 1987, in Second Conference on Faint Blue Stars, ed. A. G. D. Philip, D. S. Hayes, & J. Liebert (Schenectady: Davis), 319

Friedrich, S., Koester, D., Heber, U., Jeffery, C. S., & Reimers, D. 1999, AA, 350, 865

Goddard, B. 2004, in IDF Cookbook

Greenstein, J.L. 1984, ApJ, 276, 602

Greenstein, J.L. & Trimble, V. L. 1967, ApJ, 149, 243

Holberg, J.B., Barstow, M.A. & Burleigh, M.R. 2003, ApJS, 147, 145

Hubený, I. & Lanz, T. 1995, ApJ, 439, 875

Hunter, C., Wesemael, F., Saffer, R. A., Bergeron, P., & Beauchamp, A. 2001, in ASP Conf. Ser. 226 : 12th European Workshop on White Dwarf Stars, ed. J. L. Provencal, H. L. Shipman, J. MacDonald & S. Goodchild, 155

Jura, M. 2006, ApJ, 653, 613

Kelly, R. L. 1987, Journal of Physical and Chemistry Reference Data, Vol. 16, Suppl. No. 1

Kelly, R. L. & Palumbo, L. J. 1973 in Atomic and Ionic Emission Lines Below 2000 Angstroms – Hydrogen through Krypton (Naval Research Laboratory : Washington)

Koester, D., Rollenhagen, K., Napiwotzki, R., Voss, B., Christlieb, N., Homeier, D., & Reimers, D. 2005, AA, 432, 1025

Koester, D., Schulz, H., & Wegner, G. 1981, AA, 102, 331

Koester, D., Weidemann, V., & Zeidler-K.T. 1982, AA, 116, 147

Koester, D. & Wilken, D. 2006, AA, 453, 1051

Liebert, J., Fontaine, G., & Wesemael, F. 1987, Mem. Soc. Astr. Italiana, 58, 17

Liebert, J., Wesemael, F., Hansen, C.J., Fontaine, G., Shipman, H.L., Sion, E.M., Winget, D.E., & Green, R.F. 1986, ApJ, 309, 241

Lindler, D. 2001, in User's Guide, Far Ultraviolet Spectroscopic Explorer. Baltimore: Johns Hopkins University

MacDonald, J., Hernanz, M., & José, J. 1998, MNRAS, 296, 523.

Metcalfe, T. S. 2003, ApJL, 587, L43

Metcalfe, T. S., Winget, D. E., & Charbonneau, P. 2001, ApJ, 557, 1021

Moos, H. W. 2000, in American Astronomical Society, 197th AAS Meeting, Bulletin of the American Astronomical Society, Vol. 32, 1513

Oke, J.B., Weidemann, V. & Koester, D. 1984, ApJ, 281, 276

Pelletier, C., Fontaine, G., Wesemael, F., Michaud, G., & Wegner, G. 1986, ApJ, 307, 242

Petitclerc, N., Wesemael, F., Kruk, J.W., Chayer, P., & Billères, M. 2005, ApJ, 624, 317

Press, W. H., Rybicki, G. B., & Hewitt, J. N. 1992, ApJ, 385, 404

Provencal, J.L., Shipman, H.L., Thejll, P., & Vennes, S. 2000, ApJ, 542, 1041

Shipman, H. L. & Greenstein, J. L. 1983, ApJ, 266, 761

Shipman, H. L., Liebert, J., & Green, R. F. 1987, ApJ, 315, 239

Sion, E. M., Aanestad, P. A., & Kenyon, S. J. 1988, ApJL, 330, L55

Unglaub, K. & Bues, I. 2000, AA, 359, 1042

Voss, B., Koester, D., Liebert, J., Napiwotzki, R., Christlieb, N., & Reimers, D. 2007, AA, in press

Wegner, G. 1981, ApJL, 248, L129

Wegner, G. 1983a, ApJ, 268, 282

Wegner, G. 1983b, AJ, 88, 109

Wegner, G. & Nelan, E.P. 1987, ApJ, 319, 916

Weidemann, V. & Koester, D. 1991, AA, 249, 389

Wesemael, F., Greenstein, J. L., Liebert, J., Lamontagne, R., Fontaine, G., Bergeron, P., & Glapsey, J. W. 1993, PASP, 105, 761

Wesemael, F., Petitclerc, N., Chayer, P., Kruk, J.W., Pesant, S., & Tardif, B. 2006, in Astrophysics in the Far Ultraviolet — Five Years of Discovery with FUSE, eds. W.H. Moos, G. Sonneborn, & B.-G. Andersson, 348, 239

Wiese, W. L., Smith, M.-W., & Glennon, B. M. 1966, Atomic Transitions Probabilities, Vol. 1 (NSRDS-NBS4)

Wolff, B., Koester, D., & Liebert J. 2002, AA, 385, 995

Zuckerman, B., Koester, D., Reid, I.N., & Hünsch, M. 2003, ApJ, 596, 477

# Remerciements

Je tiens à remercier personnellement François Wesemael pour son soutien, sa patience et ses encouragements tout au long de ce projet. Nos discussions m'ont toujours éclairée et motivée et ont grandement contribué à stimuler mon interêt pour les naines blanches. Merci également à Pierre Chayer pour sa collaboration et ses commentaires.